National Library of Canada
Acquisitions and Bibliographic Services Branch
395 Wellington Street
Ottawa, Ontario
K1A 0N4

Bibliothèque nationale du Canada
Direction des acquisitions et des services bibliographiques
395, rue Wellington
Ottawa (Ontario)
K1A 0N4

Your file Votre référence

Our file Notre référence

NOTICE

The quality of this microform is heavily dependent upon the quality of the original thesis submitted for microfilming. Every effort has been made to ensure the highest quality of reproduction possible.

If pages are missing, contact the university which granted the degree.

Some pages may have indistinct print especially if the original pages were typed with a poor typewriter ribbon or if the university sent us an inferior photocopy.

Reproduction in full or in part of this microform is governed by the Canadian Copyright Act, R.S.C. 1970, c. C-30, and subsequent amendments.

AVIS

La qualité de cette microforme dépend grandement de la qualité de la thèse soumise au microfilmage. Nous avons tout fait pour assurer une qualité supérieure de reproduction.

S'il manque des pages, veuillez communiquer avec l'université qui a conféré le grade.

La qualité d'impression de certaines pages peut laisser à désirer, surtout si les pages originales ont été dactylographiées à l'aide d'un ruban usé ou si l'université nous a fait parvenir une photocopie de qualité inférieure.

La reproduction, même partielle, de cette microforme est soumise à la Loi canadienne sur le droit d'auteur, SRC 1970, c. C-30, et ses amendements subséquents.

Canada

NEARSHORE CHARACTERISTICS OF AN UNDER-ICE RIVER PLUME

By

Konstanze H. Seifert

SUBMITTED IN PARTIAL FULFILLMENT OF THE

REQUIREMENTS FOR THE DEGREE OF

MASTER OF SCIENCE

AT

McGILL UNIVERSITY

MONTREAL, QUEBEC

MAY, 1995

© Copyright by Konstanze H. Seifert, 1995

National Library
of Canada

Acquisitions and
Bibliographic Services Branch

395 Wellington Street
Ottawa, Ontario
K1A 0N4

Bibliothèque nationale
du Canada

Direction des acquisitions et
des services bibliographiques

395, rue Wellington
Ottawa (Ontario)
K1A 0N4

Your file Votre référence

Our file Notre référence

THE AUTHOR HAS GRANTED AN IRREVOCABLE NON-EXCLUSIVE LICENCE ALLOWING THE NATIONAL LIBRARY OF CANADA TO REPRODUCE, LOAN, DISTRIBUTE OR SELL COPIES OF HIS/HER THESIS BY ANY MEANS AND IN ANY FORM OR FORMAT, MAKING THIS THESIS AVAILABLE TO INTERESTED PERSONS.

L'AUTEUR A ACCORDE UNE LICENCE IRREVOCABLE ET NON EXCLUSIVE PERMETTANT A LA BIBLIOTHEQUE NATIONALE DU CANADA DE REPRODUIRE, PRETER, DISTRIBUER OU VENDRE DES COPIES DE SA THESE DE QUELQUE MANIERE ET SOUS QUELQUE FORME QUE CE SOIT POUR METTRE DES EXEMPLAIRES DE CETTE THESE A LA DISPOSITION DES PERSONNE INTERESSEES.

THE AUTHOR RETAINS OWNERSHIP OF THE COPYRIGHT IN HIS/HER THESIS. NEITHER THE THESIS NOR SUBSTANTIAL EXTRACTS FROM IT MAY BE PRINTED OR OTHERWISE REPRODUCED WITHOUT HIS/HER PERMISSION.

L'AUTEUR CONSERVE LA PROPRIETE DU DROIT D'AUTEUR QUI PROTEGE SA THESE. NI LA THESE NI DES EXTRAITS SUBSTANTIELS DE CELLE-CI NE DOIVENT ETRE IMPRIMES OU AUTREMENT REPRODUITS SANS SON AUTORISATION.

ISBN 0-612-05626-0

Canada

Abstract

Under-ice river plume data were collected in the spring of 1988 and 1990 at the mouth of the Great Whale River, Hudson Bay, Canada. Tidal analysis of tide gauge data and predicted tides shows a phase advance and amplitude decrease of the tide under continuous landfast sea ice. Current meter and echosounder measurements, as well as temperature-salinity profiles were taken within the first 2 km off-shore of the river mouth to provide a detailed picture of the nearshore plume conditions. Stable, subcritical flow conditions were observed for most of the sampling period, with the buoyant freshwater plume maintaining a depth of about 4 m almost continuously. During spring low tide (the lowest low tide), the cross-sectional area through which the river discharge must flow decreases substantially, resulting in supercritical (Froude number > 1) conditions over some periods and the formation of an internal hydraulic jump.

Résumé

Des mesures du panache sous la glace on été effectuées aux printemps des années 1988 et 1990 près de l'embouchure de la Grande rivière de la Baleine, dans la Baie d'Hudson, au Canada. L'analyse des marées prédites et des marées obtenues à l'aide d'un marégraphe démontre qu'il y a un avancement de la phase et une baisse d'amplitude des marées lorsqu'une couverture de glace océanique recouvre la baie. Des mesures de courantomètre, de profils de température et salinité, ainsi que de sondeur à ultra-sons ont été prises à l'intérieur d'une région s'étendant jusqu'à 2 km de l'embouchure de la rivière afin de fournir une image détaillée des conditions du panache près de son origine. Des conditions d'écoulement stables et sous-critiques ont été observées durant la majeure partie de la période d'échantillonnage, avec le panache d'eau douce maintenant une épaisseur d'environ 4 m au dessus de l'eau salée presque continuellement. Durant la marée basse de vive eau (la marée la plus basse), l'aire à travers laquelle la décharge de la rivière doit s'écouler décroît substantiellement, résultant en des conditions sur-critiques (nombre de Froude > 1) pendant certaines périodes ainsi qu'en la formation d'un saut hydraulique interne.

Acknowledgements

I would like to thank Claude Bélanger, Guy Millette and Paul Peltola for collecting the data at the Great Whale River, and my thesis supervisor, Professor R. G. Ingram, for his guidance and valuable advice on river plume studies.

I am grateful to Jean-Claude Croteau and Peter Galbraith for sharing their computer knowledge with me and Bernard Laval for our discussions on tides and hydraulic jumps.

To my parents, Waldemar and Helga Seifert, I am indebted for their constant support, love and understanding as well as their insightful comments and proofreading of my thesis. I would also like to thank my sister, Barbara Seifert, for her confidence in me and for her advice in cartography.

Finally, I would like to thank Stéphane Ethier for our conversations, both scientific and philosophical and for always being there when I needed him.

Funding was provided by NSERC. This research is a contribution to GIROQ and C^2 GCR.

Contents

List of Tables

List of Figures

Chapter 1

Introduction

Plumes and jets, which occur both in the atmosphere and the hydrosphere, have been studied in laboratories and in different field experiments in many parts of the world. A jet is the discharge of fluid from an opening into a large body of the same or similar fluid with the flow driven by the momentum of the discharged water. A plume is flow that looks like a jet, however, the discharged fluid has positive or negative buoyancy relative to its surroundings. For plumes, the buoyancy forces have the greatest influence on the flow. Buoyant jets also occur, in which momentum and buoyancy are important. At the source of the discharge, momentum influences the flow, while beyond this region, buoyancy forces can become more important. At a far enough distance, the jet will begin to behave like a plume (Fischer *et al.*, 1979). Under-ice river plumes have received limited attention due mainly to their remote

locations and the difficulty of sampling.

Plume studies, particularily under-ice plume studies, are important because of the biological consequences of freshwater spreading along the ice-ocean interface. Work by Gilbert *et al.* (1992) and Fortier *et al.* (1995) showed that the plume of the Great Whale River adversely affected the foraging of first feeding Arctic cod (*Boreogadus saida*) and sand lance (*Ammodytes* sp.). Feeding was reduced because freshwater ice associated with river discharge is less favourable to the growth of ice algae. Calanoid copepods graze on the ice algae, which triggers early reproduction and a better chance of survival. Their eggs are the main source of food for the first-feeding fish larvae. Also, fish larvae are visual predators. Their ability to feed depends on how much light is available for them to see their prey. The river plume water is more turbid than the ocean waters, resulting in enhanced attenuation of light, which hinders the fish from finding their food.

In the early seventies, Hydro-Québec proposed to dam several large rivers flowing into James Bay and Hudson Bay for hydro-electric power production. This provoked a series of in-depth studies of the physical and biological features of these areas. As part of the research undertaken, river plumes were investigated both in open water and under sea ice. Of particular interest were the La Grande River (Freeman, 1982; Ingram and Larouche, 1987a; Messier *et al.*, 1989) and the Great Whale River (Ingram, 1981; Ingram and Larouche, 1987b; Lepage and Ingram, 1991).

While the above studies described the shape and extent of the plumes in the offshore waters under different conditions, the work presented here focuses on the near shore aspects of the under-ice plume of the Great Whale River. The objectives of this study include a discussion of the tides and circulation in Hudson Bay and a characterization of the near-shore region of the under-ice plume.

1.1 Previous Work on Plumes and Jets

The present work focuses on the outflow of river water into a large receiving bay, so previous work on hydrological plumes is of most interest. Most studies have been made based on laboratory experiments, although field data analyses, theoretical analyses and numerical models have also been employed.

A majority of the experiments have been carried out in engineering laboratories. The lab setting allows for complete control of the outflow, the shape and size of the receiving basin, as well as the characteristics of the ambient water. Bo Pedersen (1987) describes how to build and operate a multipurpose stratified flow flume. Density differences can be produced by either using water of different temperatures or with different salinities. In another study, Kranenberg (1987) investigated two-layer stratified flow. He used an annular flume with a horizontal bottom and vertical sidewalls to study entrainment.

In lab studies, jets, rather than plumes are more often the main area of investigation. The jets can be characterized by injecting dye into the flow, projecting shadows, known as shadowgraphs, or taking photographs. Safaie (1979) looked at the mixing of buoyant surface jets over an adjustable sloping bottom. The buoyant flow of a freshwater river discharge into a salty basin often occurs over a sloping bottom, therefore, this type of experiment provides a good representation of naturally occurring events. Dye was used to follow the evolution of the jet and the patterns were recorded by a camera. His conclusion was that the characteristic geometry of a buoyant surface jet discharged over a sloping bottom is determined by the buoyancy spread, the spread due to the formation of large-scale vortices, and the spread due to turbulent mixing. However, for low densimetric Froude numbers, buoyancy is predominant, which allows lateral spreading to occur at the source.

The Froude number, a dimensionless number that describes the state of an open channel flow, is a comparison between the fluid velocity and the wave speed. When $Fr < 1$, the fluid moves slower than the wave speed and downstream conditions can affect the flow upstream, since disturbances can travel upstream. This condition is termed stable or subcritical. Unstable or supercritical conditions occur when the fluid velocity is greater than the wave speed. $Fr > 1$ and disturbances cannot travel upstream.

Baddour and Chu (1975) also considered a buoyant discharge over a sloping bottom. They observed that the behavior of the jet depended on both the upstream and downstream conditions. Their experiments also showed that the influence of the bottom slope was negligible when the slope angle is $> 25^{o}$. For less steep slopes, turbulent entrainment was generally lower than in other conditions. Lower entrainment occasionally resulted in a jet partially attached to the channel bottom. For the Great Whale River, the slope angle is low enough that, should jet conditions occur, the possibility of bottom attachment does occur, as discussed by Veilleux (1990). Chu and Jirka (1986) studied surface buoyant jets, plumes and internal hydraulic jumps in the laboratory. Shadowgraphs were used to illustrate their results. Along with the source characteristics, discharge dynamics were strongly influenced by the properties of the receiving water. Cross currents in the receiving water can deflect a jet or plume so much so that it may even attach to the downstream shoreline. In their experiments, it was also determined that when the densimetric Froude number at the source was < 3, the presence of a surface jet was not always possible since mixing could occur before the jet could develop. The formation of a plume does not appear to be affected by this criterion.

Laboratory experiments are important since they provide a controlled environment in which specific aspects of hydrological phenomena can be varied and relationships amongst the variables determined. While field measurements of hydrologic plumes

have been limited, data collection has nonetheless occurred in many regions of the world. In some of the following field studies, numerical models have been used in interpreting the data.

Garvine (1974) focused on the physical features of the Connecticut River plume that is formed in Long Island Sound (USA). The aim of the field program was to determine the horizontal distribution of the near-surface river outflow. From observations of the areal extent of the river outflow during high discharge, several important results were obtained. The outflow of the river was found to be highly variable. A great part of the variability was attributed to the strong tidal currents and the volume of fresh water discharged over the tidal cycle. Local variations of wind stress were unimportant during the experiment. As the discharge volume of the river increased, so did the horizontal area, defined by the 20 $^{o}/_{oo}$ isohaline. Once a critical discharge value was reached, the plume deepened and the horizontal area decreased. In spite of the internal densimetric Froude number being > 1, the interface between the two water layers was quite stable.

Further field studies of the Connecticut River plume were carried out by Garvine (1977). He determined that the dominant parameter governing plume formation is the ratio of fresh water volume flux to the mean tidal volume flux in the lower reach of the river. When values of this ratio are small, mixing occurs upstream of the mouth and a plume does not form. Observations of drifters and drogues in the plume region

indicated that the ambient water follows the general tidal motion along the coast and was decoupled from the plume. This suggests that the plume sits on the surface above the heavier bottom fluid and does not affect the dynamics of the lower layer in any way. Frontal zones were also observed, marked by convergence of surface drifters. On the scale of the plume as a whole, a discontinuous character of the velocity and density fields was displayed at the front since there were high contrasts in velocities, both in the parallel and normal directions between flows on either side of the front.

Using the knowledge gathered from the field studies, Garvine (1982) developed a small scale numerical plume model in which the earth's rotation was neglected. Horizontal gravitational spreading, frontal boundaries, and an ambient alongshore current were included. The frontal zone was analysed and it was concluded that the model results explained quite well the features of the Connecticut River plume. Expanding on this work, Garvine (1987) created a model which encompassed both large and small scale plumes, thus including the effects of the earth's rotation. The major goal of this work was to create a layer model that included fronts as discontinuities. Since the fronts were treated as discontinuities, their structure was not resolved but the use of approximate jump conditions maintained the mass and momentum balances. The model results showed that when rotation is not important, supercritical conditions occur throughout the plume, while for the cases in which rotation is important, subcritical conditions occur downstream despite supercritical conditions near the river

outflow.

Bowman and Iverson (1977) also studied estuarine and plume fronts. They concentrated on small scale fronts, thus excluding Coriolis effects. Field observations were made of the Hudson River plume (USA). By measuring salinity, temperature, chlorophyll *a*, ammonia, and suspended particulate matter concentrations, a three dimensional view of the plume was possible. In the coastal regions, the physical and biological effects of a river plume were found to depend upon the seasonal discharge pattens and the stability of the water column. Fronts were examined and it was found that they will only persist as long as the discharge and the receiving water are confluent.

Field work has not been limited to the Northern Hemisphere. Luketina and Imberger (1987; 1989) examined plumes and jets in Koombana Bay, Western Australia. The Cut, a man-made channel and the source of the fresh water into the bay, created a jet which transformed into a plume some distance offshore. The first of these two papers presented the general plume characteristics. They investigated the shape of the plume, associated fronts, the streamline patterns in the frontal region, and the development of instabilities. The seaward portion of the plume front was found to be quite well represented by a semicircle. The centre of this circle was defined as the virtual origin of the plume. The plume was characterized by a closed rotorlike circulation in the vertical at its leading front, associated with strong convergence ahead

of the plume. Maximum entrainment occurred at the bottom of the rotor. Further study of the same area of the plume was used to discuss the turbulence and entrainment characteristics in the plume. The plume was found to be divided vertically into a surface layer, a stable layer, a sheared mixing layer and, below the plume, a quiescent layer. The generation and collapse of turbulence was investigated in this stratified area. The surface layer and the sheared mixing layer were found to have more turbulent behaviour than the other two layers. The entrainment velocity was found to be a maximum at the leading edge and to decrease exponentially inward towards the source.

In regard to numerical modelling of plumes, Chao and Boicourt (1986) used a three-dimensional primitive-equation model with a rigid lid to study the generation of estuarine plumes. Coriolis effects were included in their analysis. The mean circulation pattern was taken to be an offshore upper layer river outflow and a landward bottom layer flow. Ocean salinity was assumed to be 35 $^{o}/_{oo}$ to dramatize the model response. This value is much larger than that found in Long Island Sound (25 $^{o}/_{oo}$ Garvine 1974) or under the Hudson River plume, (32 $^{o}/_{oo}$, Bowman and Iverson 1977). Chao and Boicourt (1986) determined that the initial injection speed from the estuary mouth had little influence on the model results. This contradicts the significance of the discharge velocity in the Froude number calculations. Higher discharge speeds would tend to produce supercritical conditions. River-forced estuarine

plumes were further investigated by Chao (1988a) using the same numerical model discussed above. In this case, Froude number analysis was performed. However, a sharp transition between subcritical and supercritical conditions was not possible because of mixing effects. Chao (1988b) next considered the effects of wind on estuarine plumes. Wind-induced mixing was found to occur during offshore as well as during landward and downwelling favourable winds. Only upwelling winds were found to enhance stratification. To complete his series of investigations on estuarine plumes, Chao (1990) looked at how these plumes might be modulated by a semidiurnal tide. Again, a three-dimensional primitive-equation model, which included the Coriolis force, was used. The rigid-lid was replaced with a free surface. One result of this analysis was that tides enhance and speed up the expansion of a river-forced plume off the mouth of an estuary.

O'Donnell (1990) created a numerical model to investigate the growth of a river plume in a basin with a steady crossflow. Included in this model were the effects of nonlinear advection, Coriolis acceleration, time dependency, mixing, friction, and a free frontal boundary. It was assumed that a strong front surrounded the plume and that this could have consequences on the flow in the plume itself. It was determined that for small scale river plumes, the direct effect of a moderate wind is of secondary importance to its evolution. However, for larger plumes the wind has a more predominant effect. If the shape of the plume was defined by the position of its fronts,

the magnitude of the crossflow only slightly modified the general plume shape. More rapid spreading occurred in the downstream direction, however the total area was only weakly affected. When the crossflow direction was changed gradually from one direction to the opposite, a basic representation of a tidal pattern was obtained. The results of this experiment suggested that once the spreading of the plume was constrained to a particular direction, mixing through shear flow instability would result if the crossflow velocity were changed. It also became apparent that whenever the tidal flow changed direction, the plume would be destroyed, and then develop and grow on the opposite side of the river mouth.

Under-ice plumes, with a solid upper boundary (i.e. continuous landfast sea ice) have rarely been studied. Freeman (1982) performed fieldwork at two major rivers flowing into Hudson Bay, Canada, the La Grande River and the Great Whale River. He observed a sharp density front 20 km offshore from the La Grande River and a sharp halocline at a depth of 3 to 4 m out to 40 km from the river mouth. From the kinetic energy distribution, it seemed that the tide modulated the river discharge rather than contributed to plume mixing. To characterize mixing conditions in the plume, he calculated the estuarine Richardson number and the plume densimetric Froude number. He found that mixing in the nearshore was only weakly dependent upon the Richardson number, but once a critical value was reached ($\sim$ 1.0) dependence on Richardson number increased significantly. From this analysis, Freeman

suggested that there are three different dynamical regions in the under-ice plume of the La Grande River. He described a thinning of the halocline interface along with a large horizontal divergence of the outflow, as well as a reduction of the flow speed within the first 5 to 10 km from the river mouth. Downward entrainment, and continued thinning of the upper layer characterized the next region which extended downstream of the first by about 25 to 30 km. This region was bounded by a plume front. Beyond this front, substantial mixing took place. Freeman used the field data to help formulate a two layer plume model. Although Coriolis effects were excluded, the surface ice layer was incorporated. Using field data for calibration, the model was used to simulate the La Grande River plume. Both the areal extent of the plume under the ice and the horizontal salinity distribution for different discharge conditions were well predicted. However, the model did not reproduce the distinct frontal region satisfactorily.

Ingram (1981) used field measurements to characterize the Great Whale River plume. Open water and ice covered conditions were considered. In both cases, the plume layer was stable with a gradient Richardson number of about 3 in open water and about 30 under a sea ice cover. During open water conditions, it was found that, when considering the Froude number, the flow was supercritical except at high tide. Subcritical conditions were found during the ice covered period, which implies that offshore events could influence flow conditions at the river mouth. While open water

conditions are such that the effects of the surface wind stress on the local surface circulation are greater than the tidal influences, the winter ice cover prevents the wind from having a direct influence. It was determined that the characteristics of the plume varied greatly between open water and ice covered conditions. The winter plume was found to be much thicker and covered a greater area than did the summer plume despite lower river discharge values in winter and early spring.

Studies of the under-ice plume of the Great Whale River were continued by Ingram and Larouche (1987b). Six different under-ice plume configurations were compared. A power law relationship, $A = aQ^b$, was found to adequately determine the effect of the river discharge, Q, on the surface area, A, of the plume. A mean entrainment velocity of $6 \times 10^{-6} cm/s$ was estimated for the January to March period. Lower entrainment rates are expected in late April and early May mostly due to increased water column stability. Downward entrainment seemed present since tidal velocities were higher below the plume than within it. The configuration of the plume, which demonstrated either radial spreading, along shore orientation, or a tonguelike intrusion, depended on several factors: time since the freeze-up, the stability of the water column and the low-frequency (5 - 10 days) coastal circulation generated by large scale atmospheric pressure forcing (see also Reynaud *et al.* (1992)). The landfast ice extent was also found to have important consequences on the plume dynamics since it influences the response to wind forcing and the tidal current strength and phase.

Studies of the vernal ice cover breakup in Hudson Bay and its effects on the upper layer dynamics were made by Lepage and Ingram (1991). Calculations of potential and kinetic energy, buoyancy fluxes and dissipation rates were made. It was found that under a complete ice cover, low turbulence levels, caused by weak circulation, promoted the expansion of the plume and resulted in highly stratified conditions in the upper 10 m of the water column. It was also shown that the ice cover has an effect on the amplitude and phase of the semi-diurnal tide. A more detailed discussion of this phenomenon can be found in Chapter 3.

The preceding parts of this chapter provided an overview of some of the plume studies previously carried out. In Chapter 2 the background theory required for the analysis of plumes and jets will be described. In Chapter 3, the study area in Hudson Bay and a description of data collection and methods will be given. Chapter 4 will include the data analysis and results. A discussion of results will be presented in Chapter 5 with the conclusion in Chapter 6.

Chapter 2

Theoretical Aspects

While plumes and jets are present in fluids that are both gaseous and liquid, the discussion here will focus solely on the hydrological case. Although they are often considered concurrently, there are significant distinctions which must be made between jets and plumes. First, a brief discussion of jets will be presented. Thereafter, a more detailed look at plumes and some aspects of the theory required for their study will be given.

Jets in the ocean are usually generated by human activity. In general, a jet occurs when a fluid is released from a small opening into a larger basin of fluid. If the two fluids have the same density, a jet will occur whose driving force is its own momentum. When the two fluids have different densities, buoyant jets form, which are influenced by both momentum and buoyancy. Jets have been studied in

many controlled laboratory experiments, as discussed in Chapter 1, and are quite well understood. As the distance from the outflow increases, all jets tend to become plumes.

Plumes are more commonly found in nature than are jets. River discharges into lakes or oceans are often plume-like. They are usually present because the outflowing water is less dense than the water in the receiving basin. The density differences are either due to dissimilar temperatures or salinities or a combination of the two. Their development and persistence is, however, only possible provided strong mixing does not occur, as discussed by Garvine (1977). While turbulent stresses, entrainment, rotational effects, as well as the characteristics of the receiving water all have important consequences on the plume, the buoyancy is the most important factor. In order to better understand plumes and plume dynamics, it is worthwhile to look at the individual characteristics and governing parameters.

2.1 Buoyancy

The buoyancy flux is defined by Fischer *et al.* (1979) as

$$B = g\frac{\Delta\rho_o}{\rho}Q = g_o'Q \tag{2.1}$$

where $\Delta\rho_o$ is the density difference between the outflowing and receiving waters at the river mouth, ρ is the density of the plume water and Q is the initial volume rate

of flow. g is the acceleration due to gravity and $g_o' = g\frac{\Delta\rho_o}{\rho}$ is the initial reduced gravity.

Although the buoyancy is often determined by the temperature of the fluid, in open ocean applications the form presented here is required since both salinity and temperature variations are important.

The spreading of the plume as it enters the receiving basin of water is due to buoyancy. The less dense plume water rises to a higher level than the surrounding water and a horizontal pressure gradient results. This gradient produces spreading of the river water over the denser basin water. If mixing between the two layers does not occur, the thickness of the plume will decrease as it expands horizontally (Bowden, 1983).

The buoyancy is dependent only on the initial reduced gravity and the river discharge. The greater the river discharge, the greater the buoyancy, and all other factors aside, the greater the horizontal extent.

2.2 Turbulence and Entrainment

Turbulence is an important element when considering plume dynamics since most fluid motions in the environment are turbulent. While it is difficult to give a precise definition of turbulence, Fischer *et al.* (1979) suggests that it can be detected as follows:

- Mass introduced at a point will spread much faster in turbulent flow than in laminar flow.

- Velocities and pressures measured at a point in the fluid are unsteady and possess an appreciable random component.

Turbulence occurs over a range of scales due to the strong nonlinearity of the equations of fluid motion at large Reynolds numbers (Fischer *et al.*, 1979). For river outflow of less dense water into more dense water, turbulence is an important source of mixing between the two layers. The greater the speed of the discharge, the greater the possibility for mixing. If the receiving basin of water is relatively deep, both vertical and horizontal turbulence are possible, and therefore mixing occurs in three dimensions. Lateral as well as vertical expansion of the plume is possible, with the amount of lateral spreading reduced to compensate for that occurring in the vertical (Bearman, 1989).

Entrainment is associated with the presence of turbulence. It is the physical transport of mass across the interface between the two layers of differing properties. Entrainment of fluid most often occurs from the non-turbulent flow into the more turbulent region. While lateral entrainment is also possible, most laboratory researchers have been concerned with the vertical exchange between stratified fluid layers. Work on entrainment has been carried out by Ellison and Turner (1959), Luketina and Imberger (1989), O'Donnell (1990), Freeman (1982) and others.

2.3 Receiving Basin

The characteristics of the receiving basin into which the river discharge enters are important in determining the transition from freshwater to the oceanic regime. Salinity differences between the river water and the basin water can be between 25 $^{o}/_{oo}$ and 32 $^{o}/_{oo}$. When crossflows are present, shear instability across the pycnocline is possible (Garvine, 1977). The depth of the basin must also be taken into account since a very shallow and/or a sloping bottom would result in bottom attachment of the river outflow (Safaie, 1979).

2.4 Richardson Number

The Richardson number is used to determine the dynamic stability of the water. It compares the stabilizing influence of density stratification to the destabilizing effect of the velocity shear. Different forms of the Richardson number have been formulated.

The *gradient Richardson number* is defined as

$$Ri = \frac{-g\frac{\delta\rho}{\delta z}}{\rho(\frac{\delta u}{\delta z})^2} = \frac{N^2}{(\frac{\delta u}{\delta z})^2} \tag{2.2}$$

(Pond and Pickard, 1983) where, $N^2 = -g(\frac{1}{\rho}\frac{\delta\rho}{\delta z})$ is the Brunt-Väisälä frequency. If $Ri \leq 1/4$, then the water is considered unstable and so mixing and turbulence are possible (Fischer *et al.*, 1979).

The *flux Richardson number* is the ratio of turbulent energy which is taken up in

vertical mixing to the buoyancy force. It was defined by Officer (1976) as

$$Ri_f = \frac{K_z}{N_z} Ri \tag{2.3}$$

N_z is the eddy viscosity and K_z is the eddy diffusivity. Neither of these two coefficients has a fixed value for a fluid. They vary both spatially and temporally. According to Officer (1976), N_z and K_z are derived quantities which are often estimated from experiments. In order to determine the flux Richardson number, details of the flow diffusion properties must be known, while the gradient Richardson number can be determined from more easily obtained physical observations.

The *estuarine Richardson number* is often used when considering the influence of river outflow on the offshore flow. (Fischer *et al.*, 1979). It is defined as

$$Ri_e = g \frac{\Delta\rho}{\rho} \frac{Q}{Wv^3} \tag{2.4}$$

where Q is the fresh water discharge, W is the channel width, v is the root-mean-square (rms) horizontal velocity and $g\Delta\rho/\rho$ is the reduced gravity. Small values of this number imply that the estuary is well mixed, while large values suggest that the estuary is strongly stratified and density currents dominate the flow. According to Fischer *et al.* (1979), the transition from a well mixed to a strongly stratified estuary occurs in the range $0.08 < Ri_e < 0.8$. Freeman (1982) used this equation, but replaced channel width W by the mean plume width, which he obtained by averaging the distances normal to the shoreline out to the frontal region of the plume.

The different Richardson numbers can all be calculated once certain basic characteristics of the flow are known. They vary as does the velocity or the river discharge.

2.5 Froude Number

The Froude number is defined as the ratio between the inertia and the gravity force (Kundu, 1990) and is given by the formula:

$$Fr = \frac{u}{\sqrt{gH}} \tag{2.5}$$

where u is the flow speed and H is the depth of the discharge channel. The flow is designated supercritical or subcritical when $Fr > 1$ or $Fr < 1$, respectively. In the case of stratified flows, the internal Froude number is more informative. The equation for the internal Froude number is

$$Fr_i = \frac{u}{\sqrt{g'H}} \tag{2.6}$$

(Kundu, 1990), where g in equation 2.5 has been replaced by g', the reduced gravity as defined earlier. Fischer *et al.* (1979) replace u in this equation by the ratio Q/A where Q is the discharge of freshwater and A is the cross-sectional area of the channel. They refer to this ratio as the freshwater discharge velocity and use the term "bulk densimetric Froude number" to designate Fr_i in this formulation.

Chapter 3

The Physical Setting, Data Collection and Methods

3.1 Study Area

Hudson Bay, located in the east central region of Canada, is a salt water basin with an area of 819 000 km^2. Hudson Strait connects the bay to the Atlantic Ocean while Foxe Channel provides a link with the Arctic Ocean, while James Bay is joined to it in the south (Figure 3.1). Despite its vast areal extent, it is, in fact, quite shallow, with an average depth of only 125 m and a maximum depth of about 270 m (Prinsenberg, 1987; Freeman, 1982). Surface salinity values during the ice covered period in southeast Hudson Bay are typically 29 $^{\circ}/_{oo}$ in mid-April (Ingram and Larouche, 1987b). Bottom

salinity values increase to 33 $^{o}/_{oo}$ at the deep oceanic inflow in the northern part of the bay (Freeman, 1982). For the first four to five months of the year, Hudson Bay is covered by a 1 to 1.5 m thick ice cover which typically breaks up in mid-to-late May. The ice is usually of the landfast type in the southeast part of the bay (Larouche and Galbraith, 1989).

The Great Whale River, with its mouth located at $55^{o}16'N$ and $77^{o}48'W$, is one of the major sources of freshwater into Hudson Bay. A sandbank is situated just offshore of the river mouth, resulting in water depths of about 2 m. Depths fall to 60 m within two kilometers from the shore. The freshwater discharge of the Great Whale River fluctuates seasonally and interannually, ranging from 100 m^3/s to 2000 m^3/s. The mean annual discharge is around 600 m^3/s (Lepage and Ingram, 1991). Spring discharges (May-June) are the highest, since melting ice and snow rapidly increase the freshwater input to the river. Figure 3.2 shows the discharge values for 1988, 1989 and 1990. Annual and interannual variations can clearly be seen.

3.2 Circulation and Tides in Hudson Bay Under an Ice Cover

The general circulation in Hudson Bay is counter clockwise resulting from winds, Arctic surface ocean waters entering from Foxe Basin, and freshwater input from

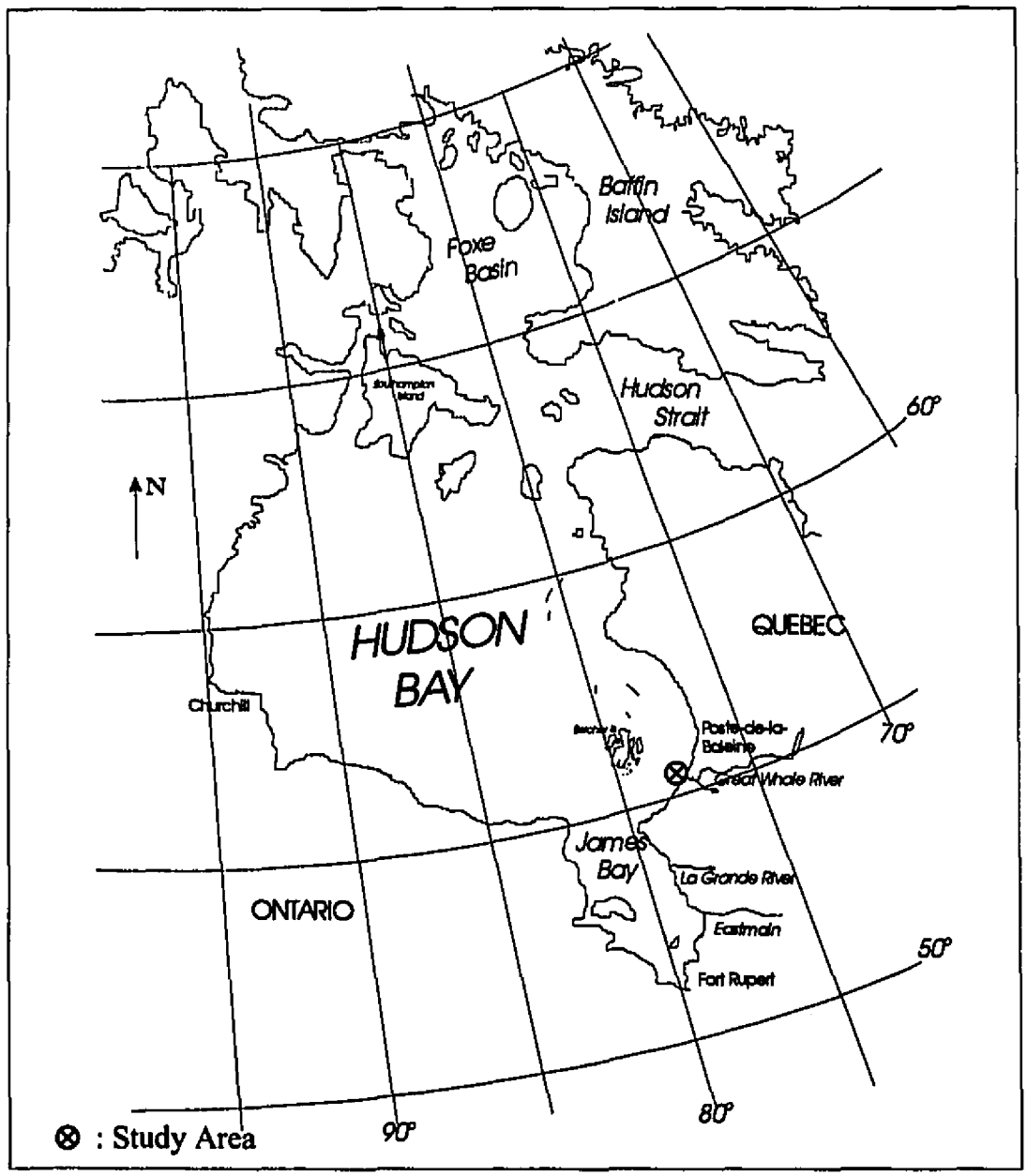

Figure 3.1: Map of Hudson Bay. The Great Whale River is at $55°16'N$ and $77°48'W$.

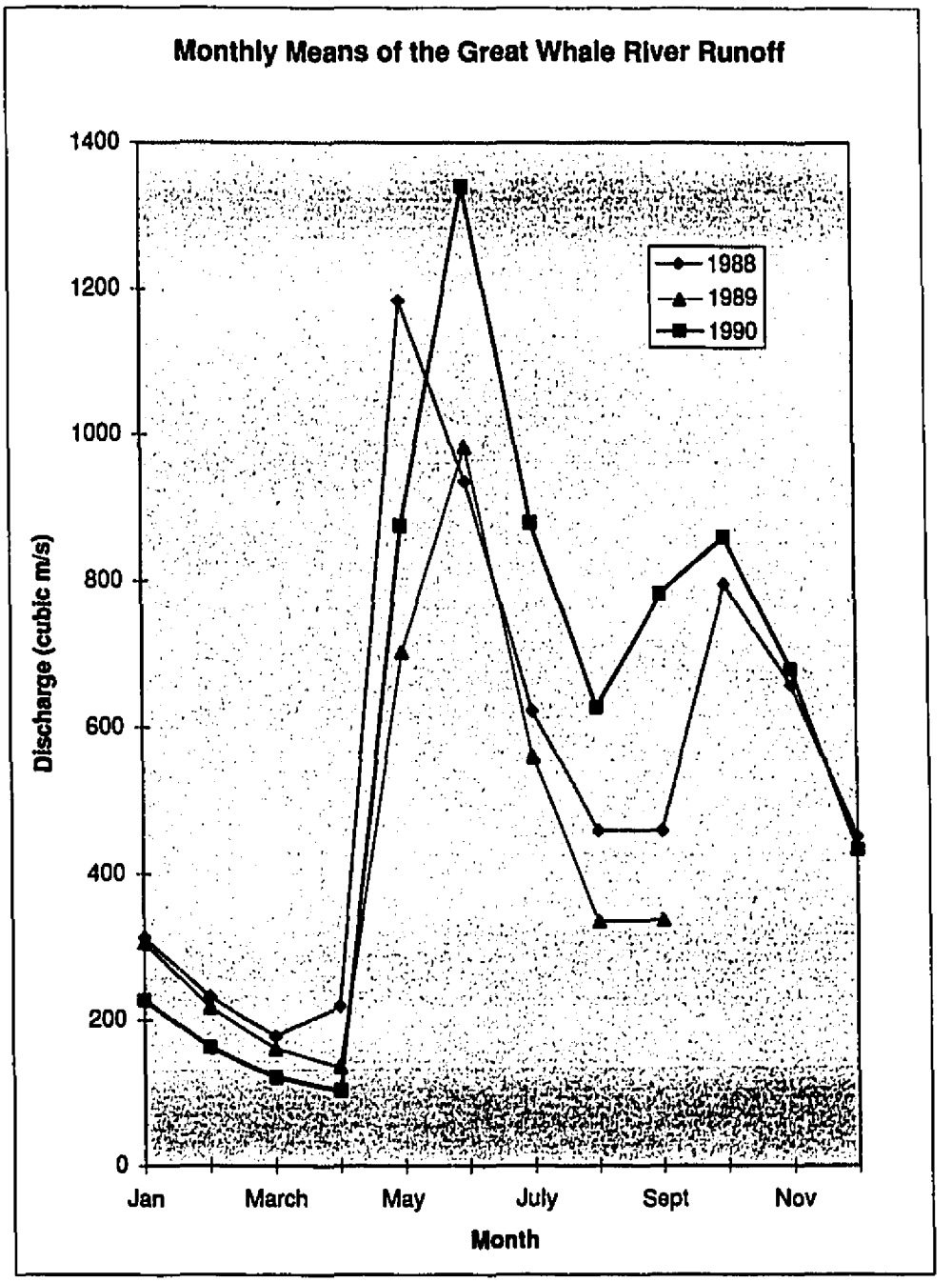

Figure 3.2: Mean monthly Great Whale River runoff for 1988,1989, and 1990. (Source: Ministère de l'Environnement du Québec.)

rivers (Prinsenberg, 1987). Prinsenberg and Freeman (1986) determined that the major portion of the current energy is associated with the tides.

A tide gauge was deployed in the spring of 1988. However, equipement malfunction resulted in an unreliable data set. Therefore, only tidal predictions were available. The predicted tide was calculated using the Canadian Tide and Current Tables produced by the Department of Fisheries and Oceans (DFO) (1988). The method involves taking actual tide gauge data collected at specific ports over long periods and using this information to predict the tide using harmonic analysis. The time and height of the high and low tides are determined. To calculate the tide height at times other than high or low tide, an interpolation must be made, with the assumption that the tidal curve is a simple cosine curve. In the description given on their technique, seasonal variations are not taken into consideration. Only data collected under ice free conditions are used to determine tidal constituents.

In 1990, a tide gauge was deployed at $55°28'N$ and $77°52'W$. The water depth is over 100 m at this location. Significant readings were taken from April 21 to May 11. After May 1, however, the high tide values were no longer correct, due to a defective pressure sensor in the instrument. Figure 3.3 shows the tidal height observations obtained from this instrument. The low frequencies were filtered out from the original signal in order to eliminate fluctuations due to passing weather systems, and the signal mean and trend were removed. From analysis of this tidal height

data, it was determined that the semi-diurnal tidal component is predominant, with other constituents, such as the diurnal component, more than an order of magnitude smaller.

The predicted tide (Canadian Tide and Current Tables, 1990) was also calculated for 1990 (Figure 3.4). The neap (minimum range) and spring (maximum range) tides can clearly be seen. Figures 3.5 and 3.6 show the predicted and the actual tides from April 21 to May 1, which corresponds to the time when the best actual tide data was collected. When comparing the two graphs, it becomes apparent that there is some discrepancy between the actual and the predicted tide. To investigate in greater detail the differences between the two, a smaller time period was plotted and is shown in Figure 3.7. When comparing the curves, it is evident that the actual tide has smaller amplitudes by $\sim$ 22 % and is advanced by about 30 minutes compared to prediction. A possible explanation for this phenomenon follows:

The M2 (principal lunar semi-diurnal) tide enters from Hudson Strait and progresses counter-clockwise around Hudson Bay as a Kelvin wave (Freeman, 1982; Prinsenberg, 1987). Two amphidromic points, (locations of little or no tide), occur in Hudson Bay as the offshore components of the Kelvin wave interfere and cancel each other out as discusses by Prinsenberg and Freeman (1986) (Figure 3.8 from Forrester (1983)).

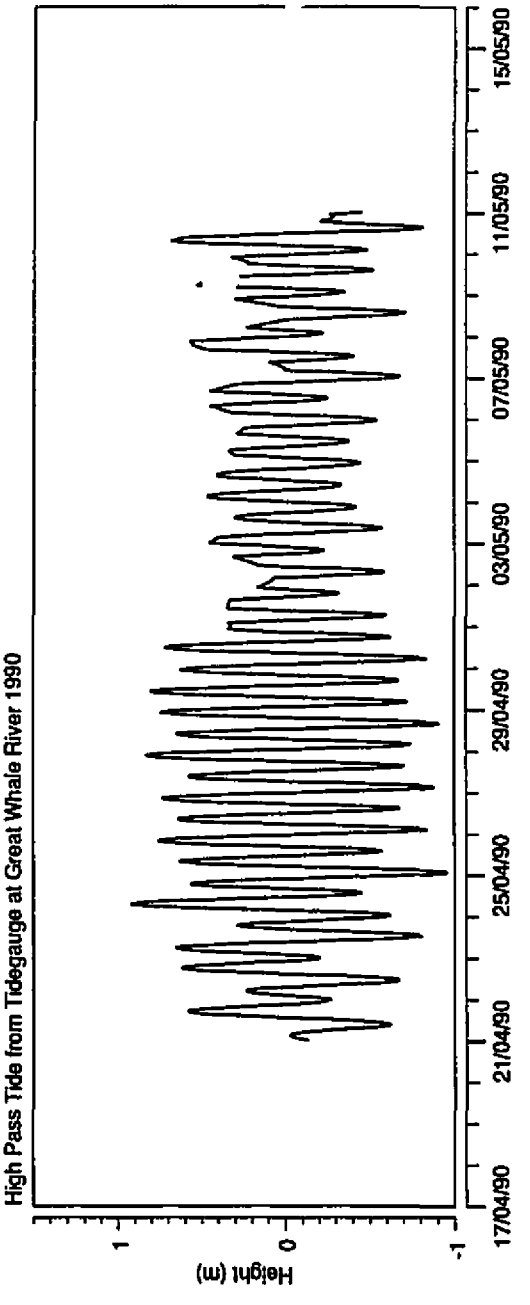

Figure 3.3: Tidal observations for 1990 from the tide gauge located at $55°28'N$ and $77°52'W$.

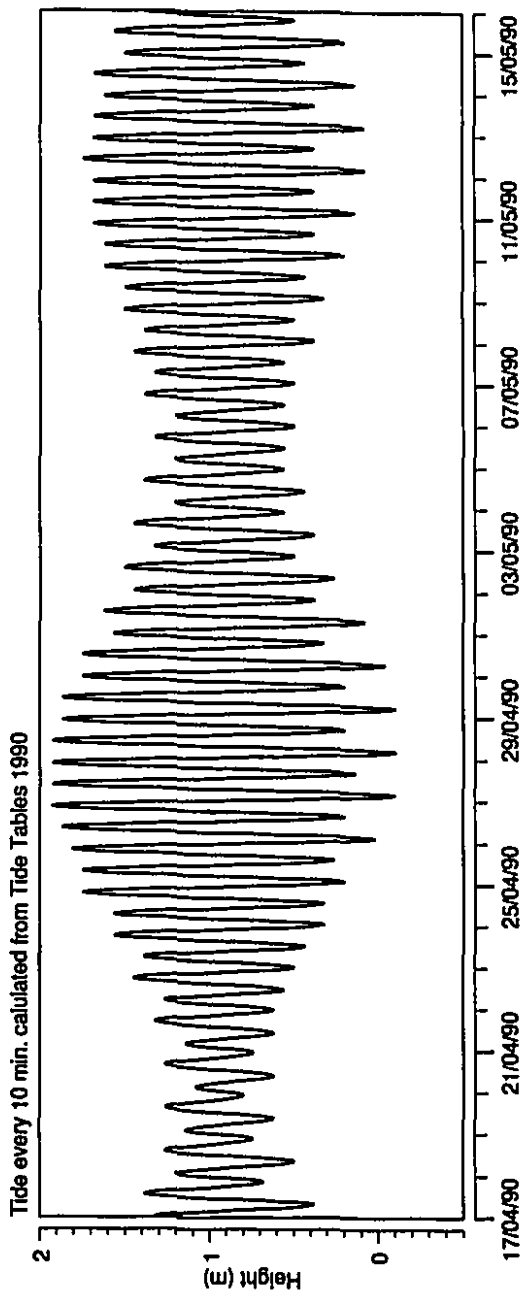

Figure 3.4: Predicted tides for 1990.

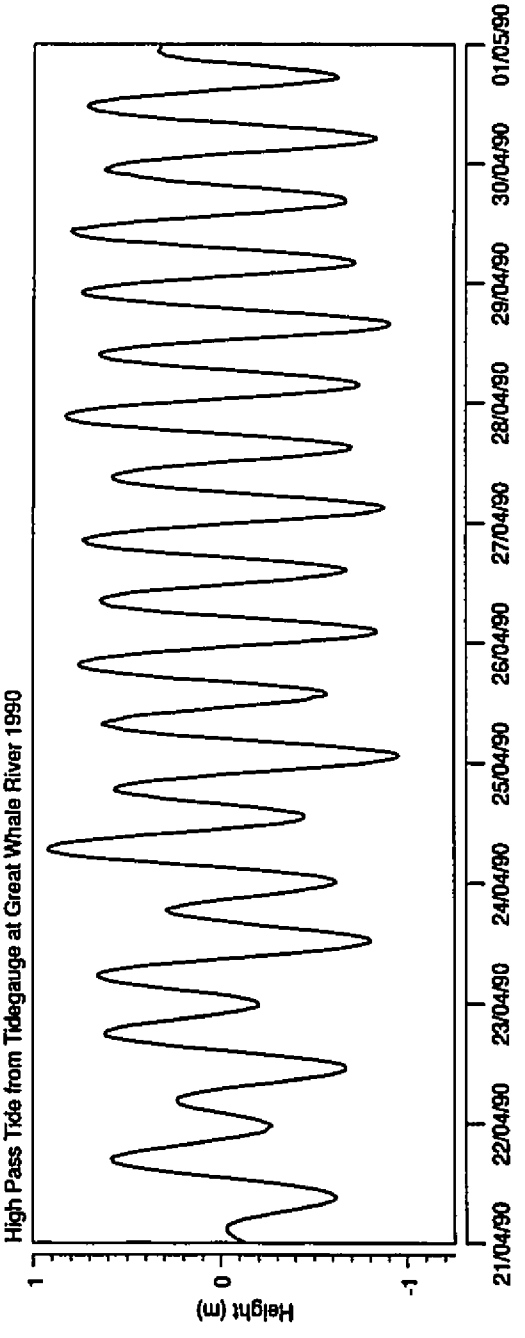

Figure 3.5: Tidal observations between April 21 amd May 1, 1990.

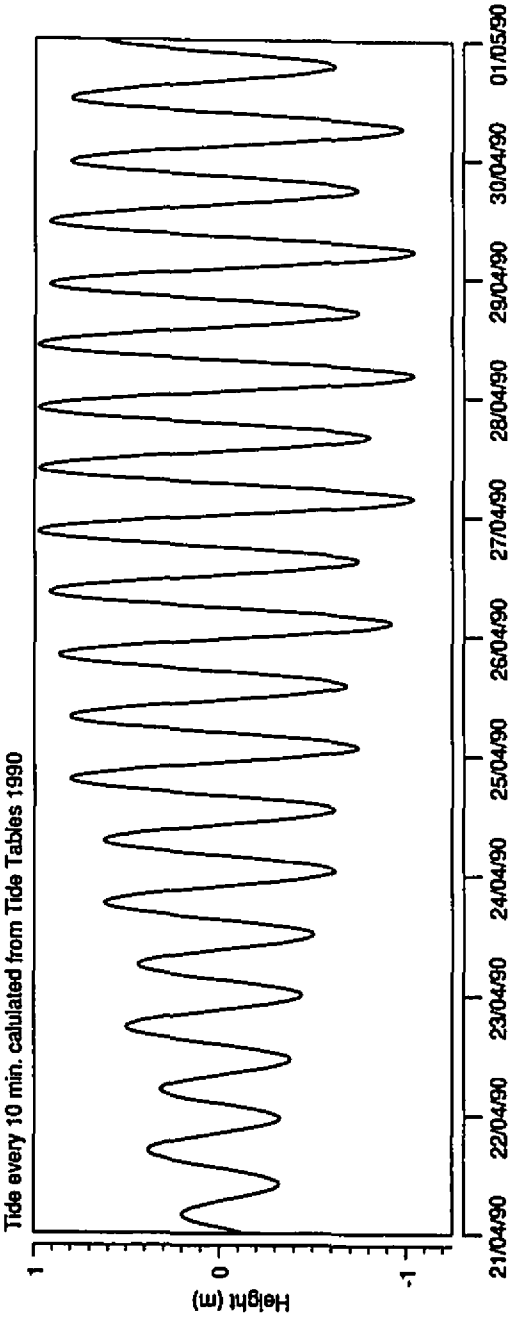

Figure 3.6: Predicted tides between April 21 and May 1, 1990.

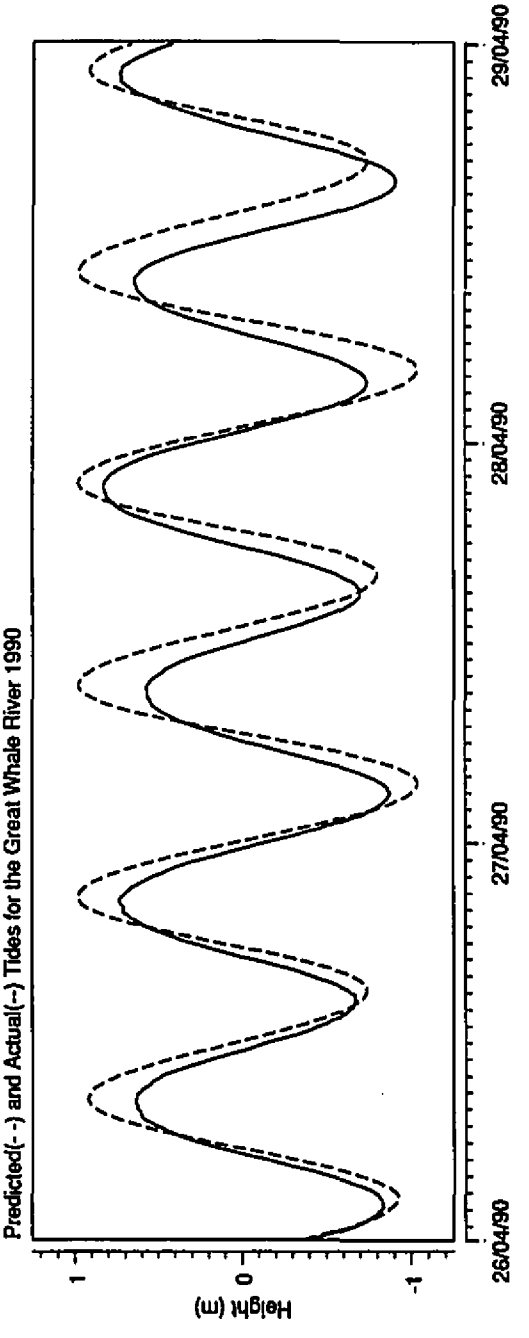

Figure 3.7: Comparison of predicted and observed tides from April 26 to 28, 1990.

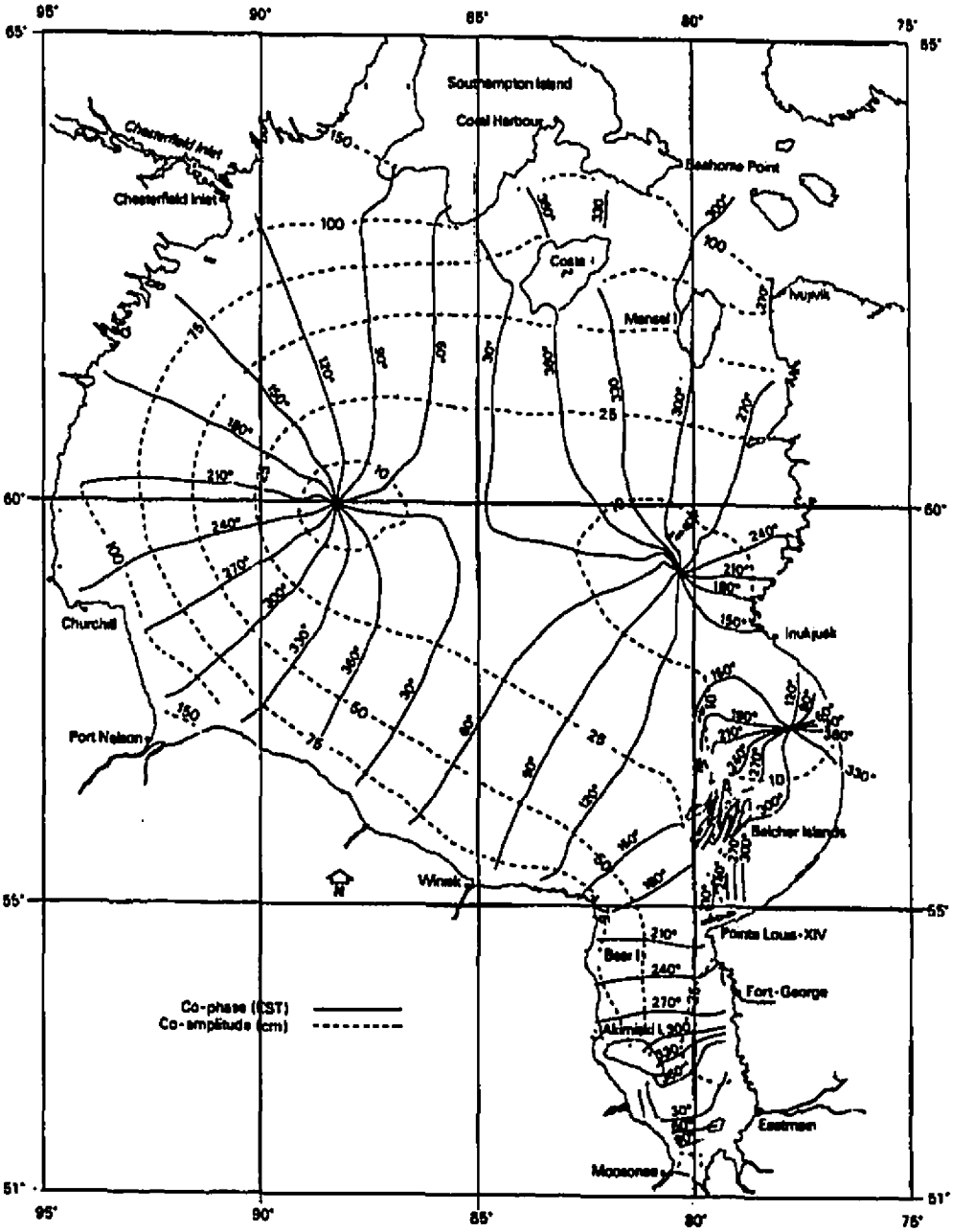

Figure 3.8: Winter locations of amphidromic points in Hudson and James Bays (adapted from Forrester (1983)).

Godin (1986) looked at the modification of the tide due to an ice cover by collecting data in Hudson Bay, James Bay and the Arctic Ocean. From this analysis he determined that while seasonal variations in the tide due to an ice cover did not occur at stations lying around the perimeter of the ocean or connected to it by deep channels, shallower locations, such as Hudson Bay and James Bay did experience tidal changes. Prinsenberg (1988) further investigated the effects of an ice cover on the tides in Hudson Bay. He found that the amplitude decreased and the phase advanced during the ice covered season, similar to what was found in this analysis at the Great Whale River and by Lepage and Ingram (1991). Prinsenberg concluded that the incoming waves, which reflected off the western coast of Hudson Bay propagated eastward parallel to the southern shore. Due to the increased friction caused by the ice cover, the amplitude of the reflected waves was smaller relative to the incident waves. This resulted in the two open water amphidromic points moving further southward, since the pattern results from a combination of the incident and reflected waves. This results in one seeing more of the incident wave than the reflected wave in Hudson Bay in the winter time.

The predicted tide at the Great Whale River was calculated using data from the reference station at Sand Head in James Bay. There is no distiction in the methods used to predict the tides during the ice free or ice covered periods of the year. This fact explains the discrepency between the predicted and actual tides at the Great

Whale River. Thus, care must be taken when using predicted tides for ice covered regions.

3.3 Data Collection and Methods

The research presented here focuses on data collected offshore of the Great Whale River between April 21 and May 6, 1990. Data collected from April 23 to May 7, 1988 at the Great Whale River will also be used. A continuous landfast ice cover of about 1.5 m on Hudson Bay provided a solid working platform for the field work in both years. Five sampling stations, denoted L1 to L5, were set up in a nearly straight line offshore from the river mouth. Their locations are shown in Figure 3.9. At a distance of 1 km offshore, the station closest to the river mouth, L5, had a maximum depth of 3.5 m, while the farthest station, L1, was situated 900 m offshore of L5, in waters of 30 m depth. Table 3.1 lists distances between the stations and the river mouth and the water depth at those locations.

Distance from river mouth and station water depth		
Station	**Distance (m)**	**Depth (m)**
L1	1900	27.0
L2	1750	16.0
L3	1480	10.0
L4	1180	4.0
L5	1000	3.5

Table 3.1: Distances between stations L1 to L5 and the river mouth and station water depth.

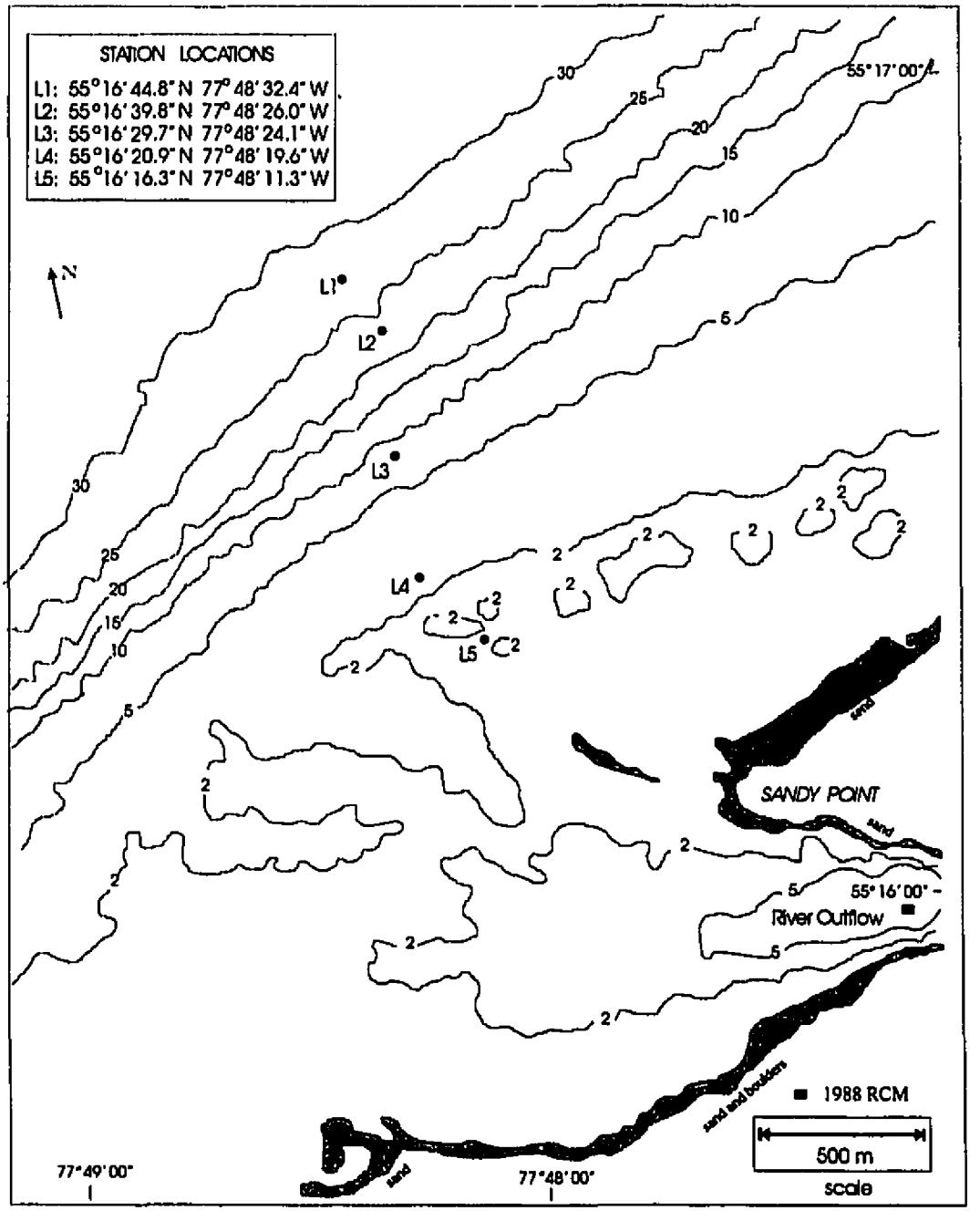

Figure 3.9: Locations of the five data collection sites and the near-shore bathymetry at the mouth of the Great Whale River. Bathymetry was obtained from uncorrected hydrographic survey by Canada Centre for Inland Waters.

Several types of measurements were taken during the sampling period. All instruments were moored or deployed from the ice surface. Conductivity-temperature-depth (CTD) profiles were taken regularly at the five stations, L1 to L5. A Seacat SBE19 instrument was used. Its precision is given in Table 3.2. In total, there were 182 profiles taken between April 24 and May 6, 1990, with twice as many at station L2 than at any of the other four.

Seacat SBE19 CTD profiler	
temperature	$\pm 0.01^{o}C$
conductivity	$\pm 0.01 mmho/cm$
depth	$\pm 0.3m$

Table 3.2: Precision of the conductivity-temperature-depth instrument.

Aanderaa RCM7 current meters were located at stations L1, L3 and L4. The precision of these instruments is given in Table 3.3. Measurements were taken every two minutes from April 25 to May 7, 1990. Two RCM were located at L1, at depths of 2.8 m and 6.6 m from the surface. At L3, the instruments were placed at depths of 2.1 m and 6.0 m. Only one RCM was located at L4 at 3.7 m from the surface.

Echosounder readings were taken at specific times during the 1990 field study using a Ross SL-600C echosounder with a frequency of 103 kHz. Profiles were taken at L1 from 17:30 on April 29 to 7:30 on April 30, at L2 from 17:00 on April 27 to 10:30 on April 28 and again from 16:00 April 30 to 11:30 on May 1 and at L3 from 17:30 on April 28 to 6:00 on April 29.

RCM7 current meter	
conductivity	$\pm 0.025 mmho/cm$
temperature	$\pm 0.1°C$
depth	$\pm 1.0m$
speed	$\pm 1.0cm/s$
direction	$\pm 5°$

Table 3.3: Precision of the Aanderaa Savonius rotor current meter.

From April 18 to May 1, 1988, an RCM was placed at the mouth of the Great Whale River. Data was collected every ten minutes, providing measurements of the river outflow velocity.

Chapter 4

Data Analysis and Results

Using moored current meter records, conductivity-temperature-depth profiles, echosounding and tide gauge measurements, the nearshore characteristics of the under-ice plume were determined. The analysis and results of the data collected at the Great Whale River in 1988 and 1990 are presented here.

4.1 Outflow Velocity

In 1988, an Aanderaa RCM7 current meter (RCM) was deployed at the Great Whale River mouth upstream of the river sill, providing a continuous data set of the river velocity from April 18 to May 1. Figure 4.1 shows the u and v components of the velocity along with the predicted tide curve and the river discharge values obtained from the Ministère de l'Environnement du Québec. The channel direction(CD) was

taken as 260°, which resulted in the u component of the velocity representing the along channel Great Whale River outflow. As was discussed above, there is some discrepancy between the actual tide and the predicted tide. However, the general pattern is still useful in explaining, in part, the observed fluctuations for the u velocity. The spring and neap tide variations can be easily seen, as well as the increasing flow magnitudes towards the end of the sampling period. This resulted from the increasing river discharge. A harmonic analysis of the current velocity was performed and compared to the to the predicted tide. For the M2 tidal constituent, the maximum positive u velocity will occur 3.6 hours after the predicted high tide. It should be noted that the current velocity record was the minimum length to do a harmonic analysis of the M2 component.

In 1990, a current meter placed near the same location was lost during spring breakup. In order to approximate the outflow velocity for 1990, the single-velocity method for measuring discharge, discussed by Strilaeff and Bilozor (1973) was used. The velocity *(u)* is related to the river discharge *(Q)*, and the cross-sectional area *(A)* by

$$u = \frac{Q}{A} \tag{4.1}$$

The river discharge data for the time periods studied in 1988 and 1990 are given in Figure 4.2. The source of this data is the Ministère de l'Environnement du Québec. Considerably larger spring discharge values occurred in 1988 than did in 1990.

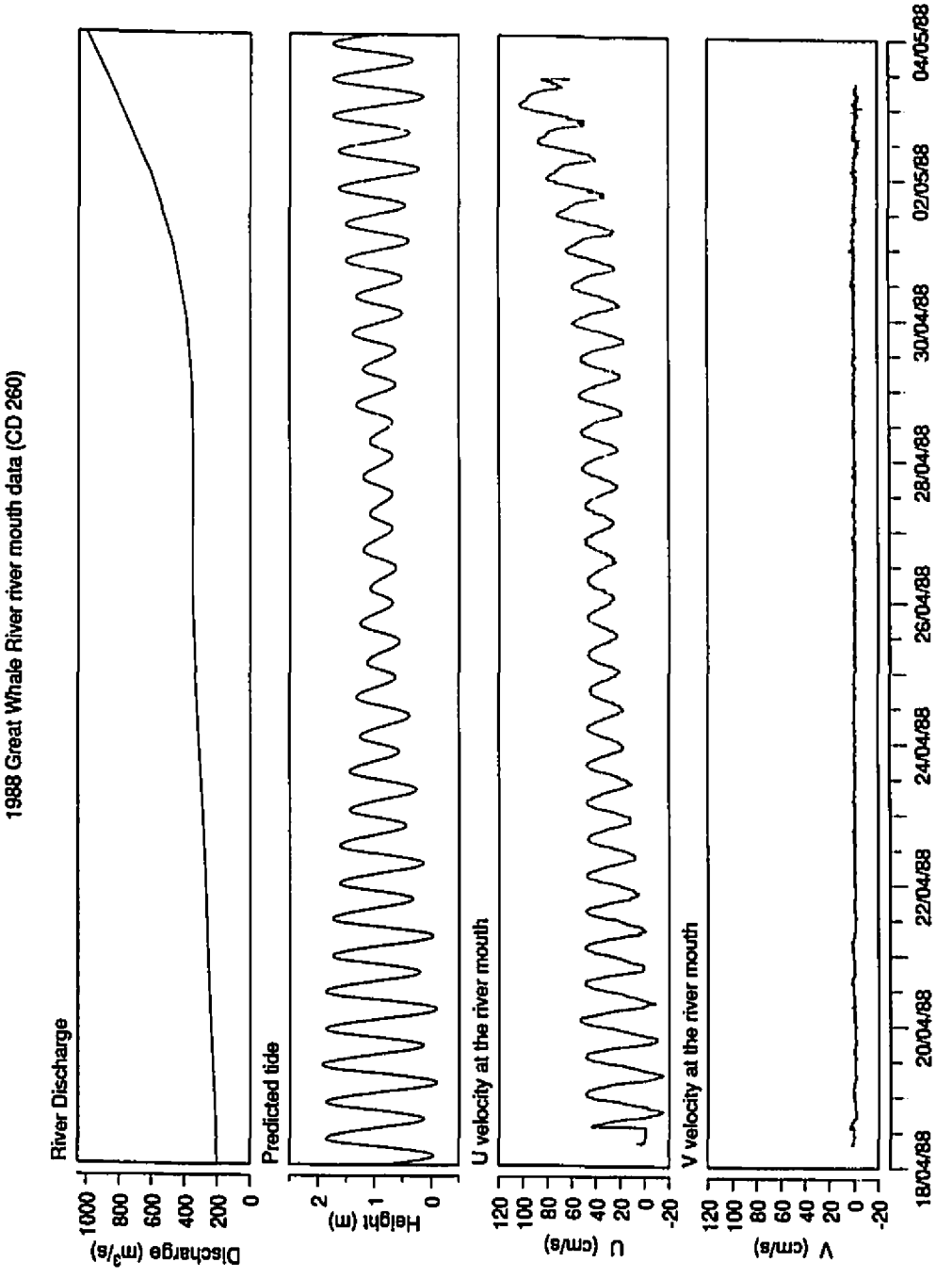

Figure 4.1: Circulation at the mouth of the Great Whale River in 1988. u and v velocity components are obtained from the RCM instrument at a depth of 4.5 m. Tides are predicted using the Canadian Tide Tables (DFO) and river discharge information was obtained from the Ministère de l'Environnement du Québec.

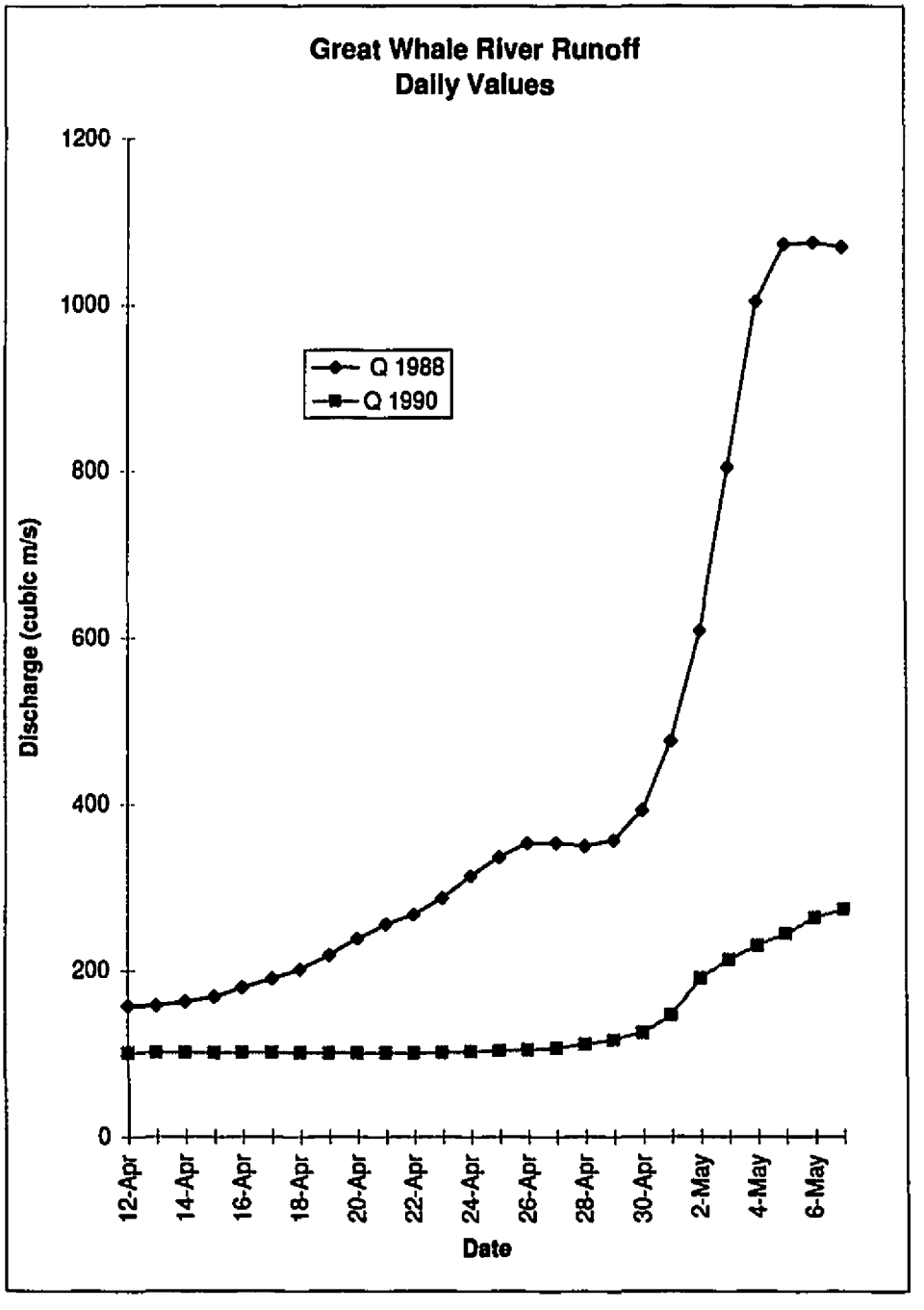

Figure 4.2: Great Whale River runoff for the study periods in 1988 and 1990 (Source:Ministère de l'Environnement du Québec).

The cross-sectional area was determined from bathymetric charts of the river obtained from an uncorrected hydrographic survey undertaken by the Canada Centre for Inland Waters as well as from the Canadian Hydrographic Service bathymetric charts. At the mouth of the Great Whale River, a sand ridge is usually formed. While its exact size and location may vary slightly from year to year, the data obtained from these two hydrological surveys are considered accurate representations of the small scale bathymetry occurring in 1988 and 1990. This is the shallowest, although not the narrowest, part of the river mouth. When taking into consideration the ice layer and the increase and decrease in height that occurs at high and low tides, the area through which the water flows can be calculated over the tidal cycle. The discharge area and outflow velocity for spring and neap high and low tides are given in Table 4.1.

1990 River Mouth Conditions			
	Q(m^3/s)	A(m^2)	u(m/s)
Spring Tide			
High April 28	110.5	2743.1	0.04
Low April 28	110.5	426.0	0.26
Neap Tide			
High May 4	229.5	2160.3	0.11
Low May 4	229.5	908.2	0.25

Table 4.1: Discharge, cross-sectional area and velocity at the Great Whale River mouth in 1990

The cross-sectional area decreases considerably at low tide, being between one half and one quarter as large as during high tide.

4.2 Echosounder Data

At the times the echosounder was deployed, measurements were taken continuously for over 12 hrs. These recordings indicate that the pycnocline depth varied with time. Figure 4.3 shows the difference from the mean of the distance between the surface and the pycnocline and the difference from the mean of the total depth of the water column for one of the four periods during which soundings were taken. Values were taken every half hour to plot these curves. Positive values represent deeper or thicker surface layers, while negative values represent shallower or thinner layers. The positive and negative depth values correspond to high and low tide respectively. The pycnocline varies less ($\pm$ 0.4) than the depth of the water column. The pycnocline fluctuations are negatively correlated with tide height, giving a correlation coefficient of -0.80. This suggests that at low tide the pycnocline is deeper than at high tide for the particular period under investigation. In other words, the fresh water layer is thicker during low tides. Since depth variations are observed, the sea-ice, while being considered landfast, does move up and down elastically with the tides. For the other stations investigated, maximum pycnocline depths were observed between 3:00 and 3:30 April 29, 1990 at L3 and at the same time on April 30, 1990 at L1.

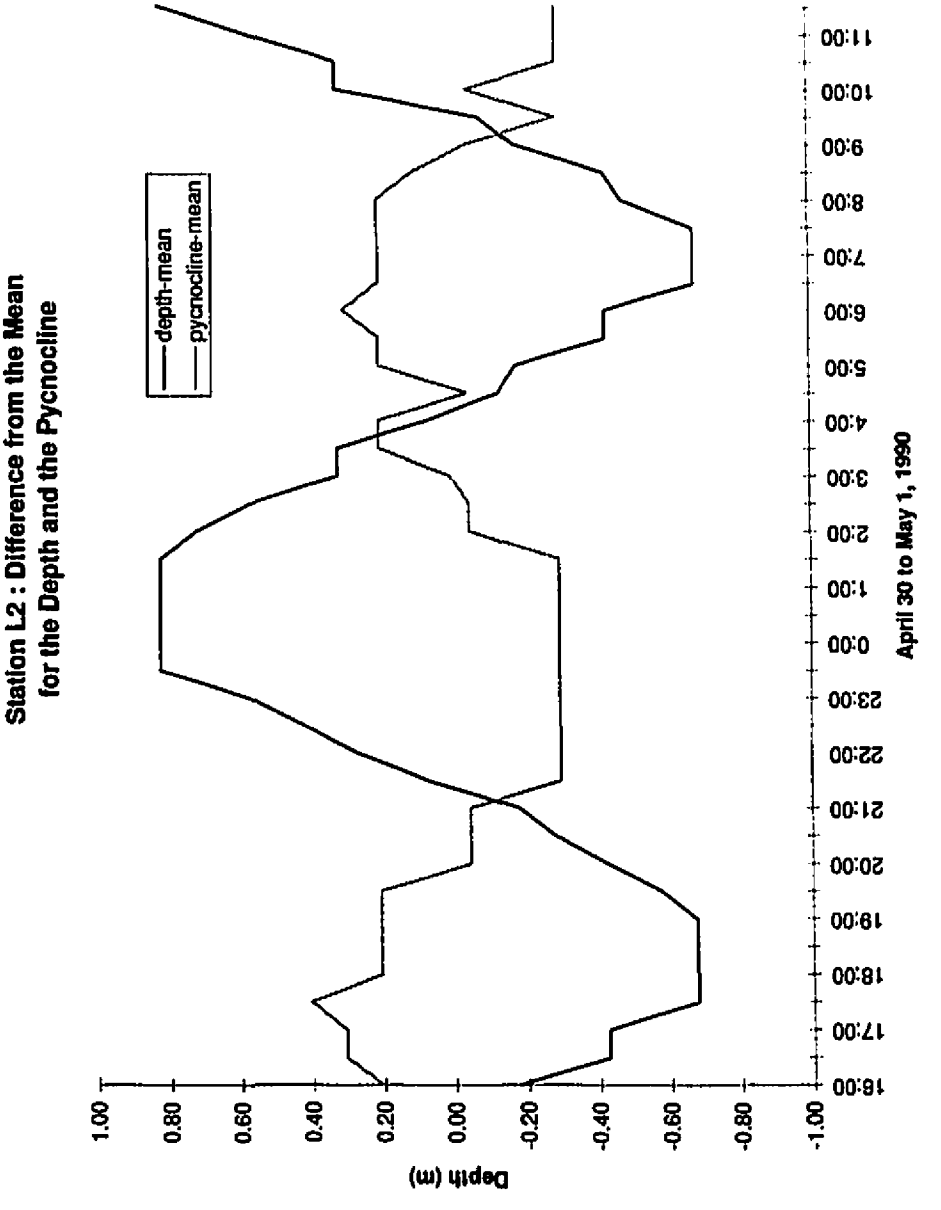

Figure 4.3: Echosounder data at station L2 on April 30 and May 1, 1990. Difference between the mean pycnocline depth and the local water column depth.

4.3 RCM Data

From the data collected with the five RCM instruments, the speed, direction, u and v components of the velocity, the temperature, and salinity, could be determined. Figures 4.4, 4.5, 4.6, 4.7 and 4.8 show the salinity, temperature, and u and v velocity components for the time period data were collected. The following observations can be made.

The upper level instruments are in the freshwater plume region since the salinity values are 0 $^{o}/_{oo}$, while those at around 6 m depths are within the saltier Hudson Bay water. The salinity values for the deeper location measured at stations L1 and L3 (Figures 4.5 and 4.7) are between 26 and 27 $^{o}/_{oo}$ almost continuously. However, between April 29 and 30 at L1 and in an even more pronounced fashion between April 28 and 30 at L3, there was a decrease of the salinity over a certain period. For L3, there was also an increase in the temperature. Figure 4.9 and 4.10 show these periods with an expanded scale. At L1, salinity decreases to 24.69 $^{o}/_{oo}$ at 2:45 and down to 24.58 $^{o}/_{oo}$ at 15:36. On April 30, there are again fluctuations with values reaching 25.30 $^{o}/_{oo}$. The fluctuations are even more pronounced at station L3 with a lowest daily value of 20.04 $^{o}/_{oo}$ recorded on April 28 at 14:18, 17.85 $^{o}/_{oo}$ at 3:08 on April 29 and 24.67 $^{o}/_{oo}$ at 4:02 on April 30.

The temperature curves show that the plume is slightly above $0^{o}C$ while the Hudson Bay water is about -1^{o}C (Figures 4.4, 4.5, 4.6, 4.7 and 4.8). Diurnal fluctuations

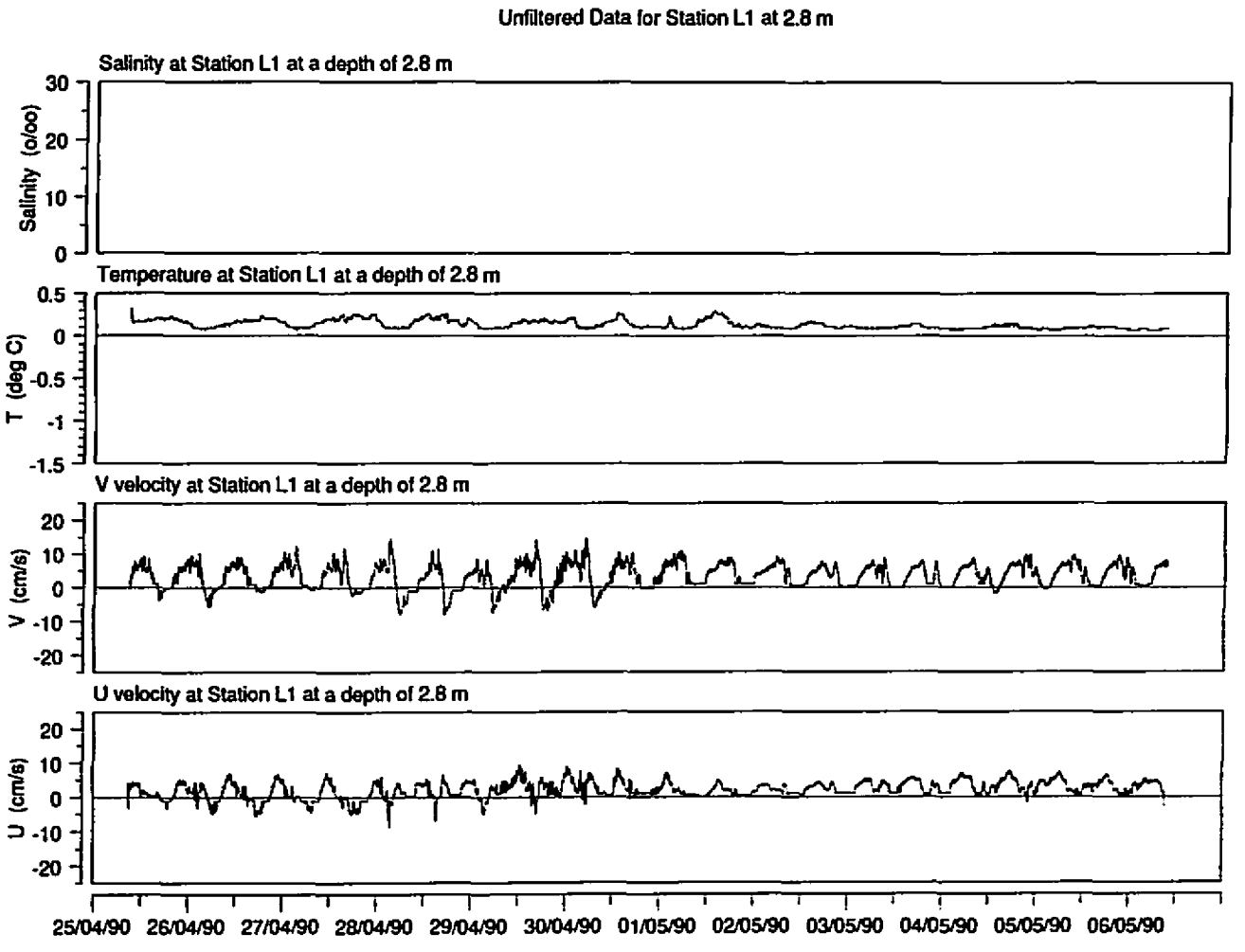

Figure 4.4: Upper level RCM data at station L1 (2.8 m depth).

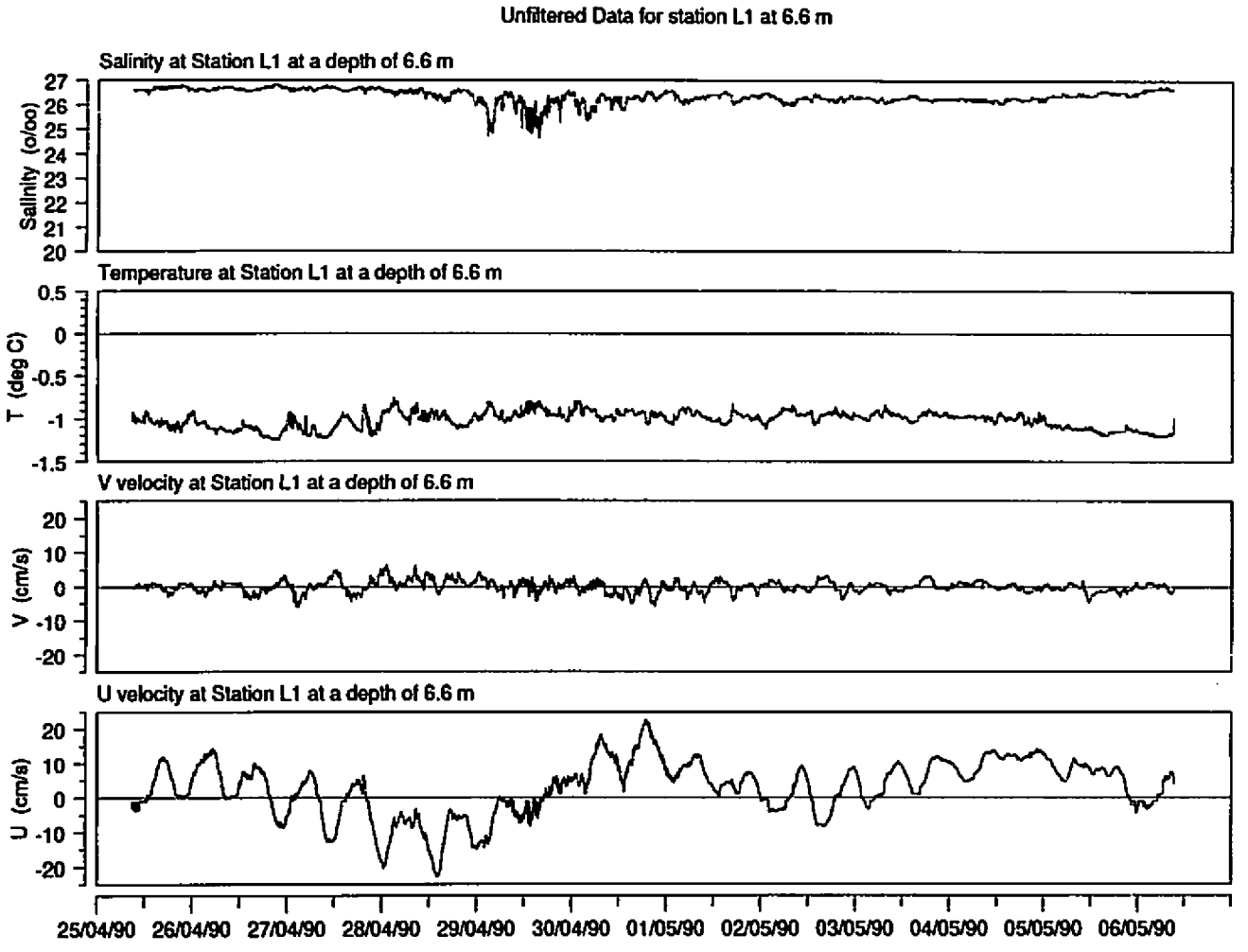

Figure 4.5: Lower level RCM data at station L1 (6.6 m depth).

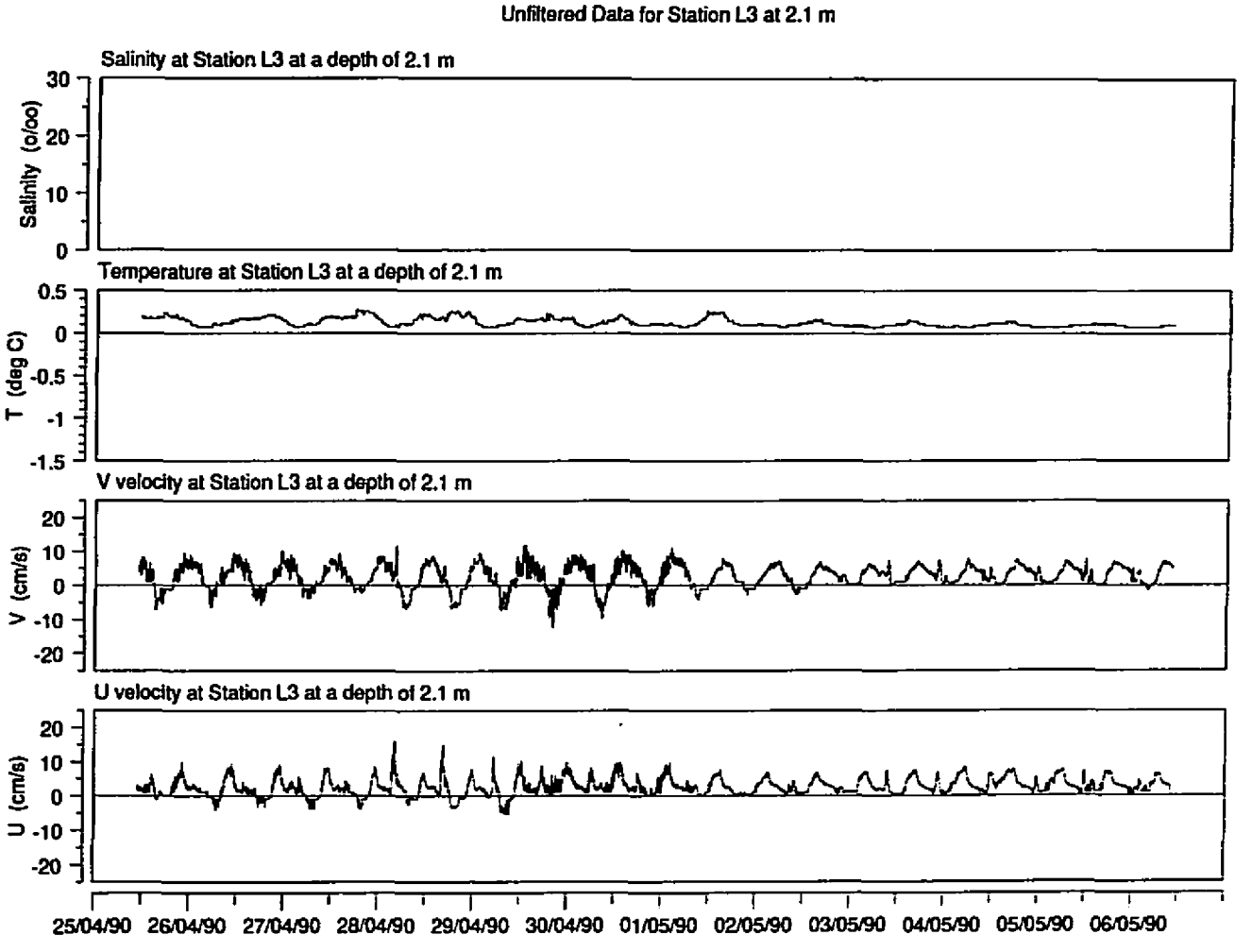

Figure 4.6: Upper level RCM data at station L3 (2.1 m depth).

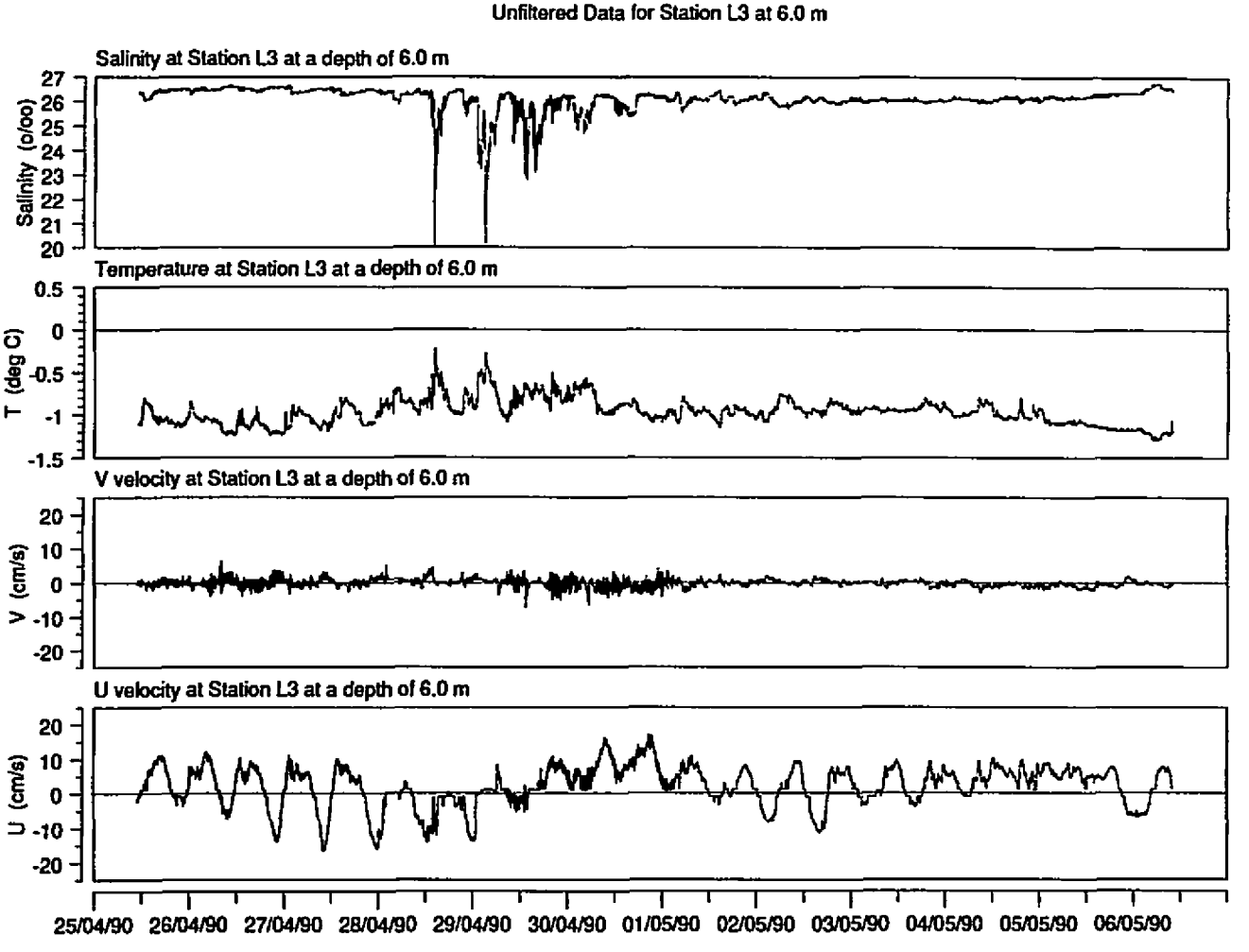

Figure 4.7: Lower level RCM data at station L3 (6.0 m depth).

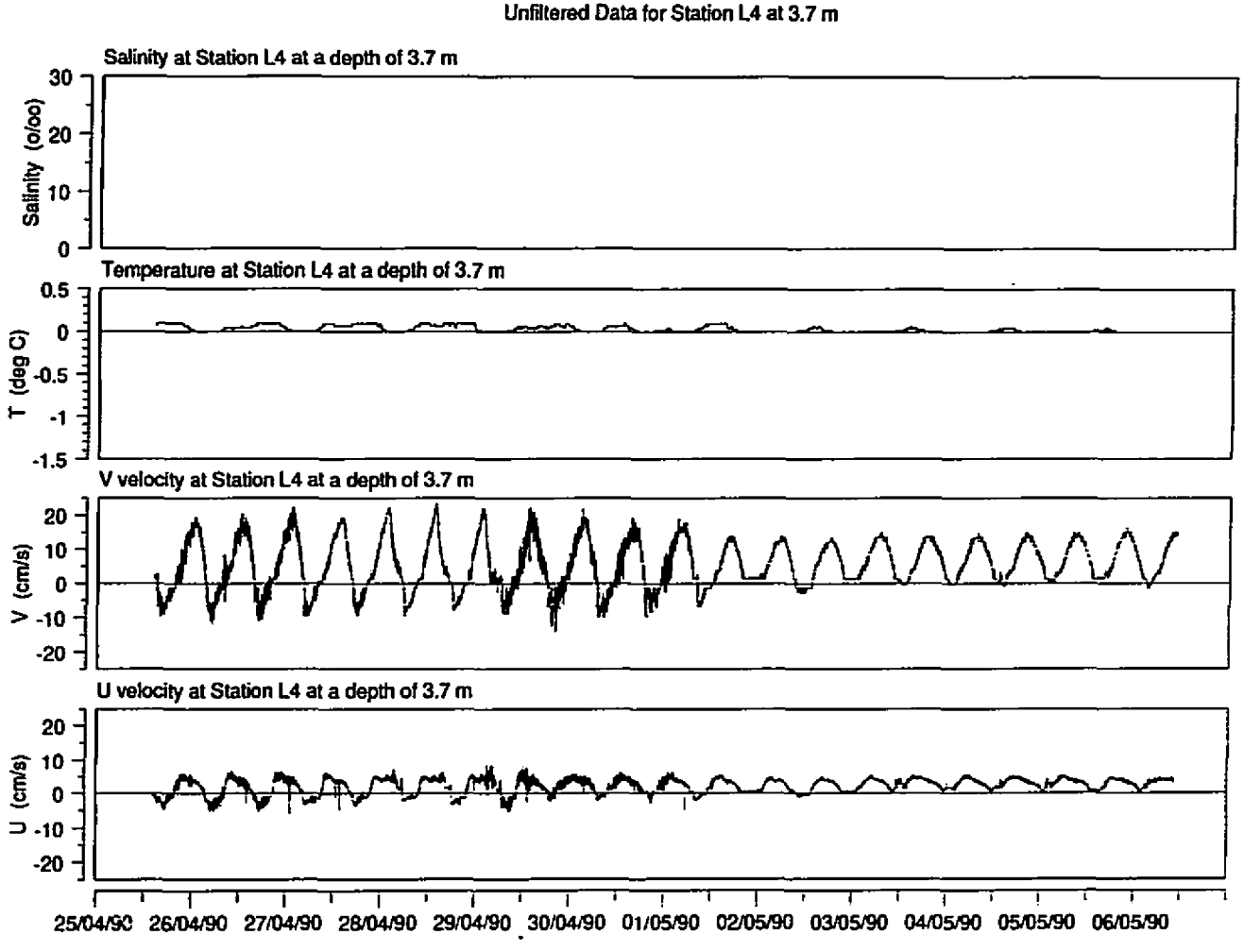

Figure 4.8: Upper level RCM data at station L4 (3.7 m depth).

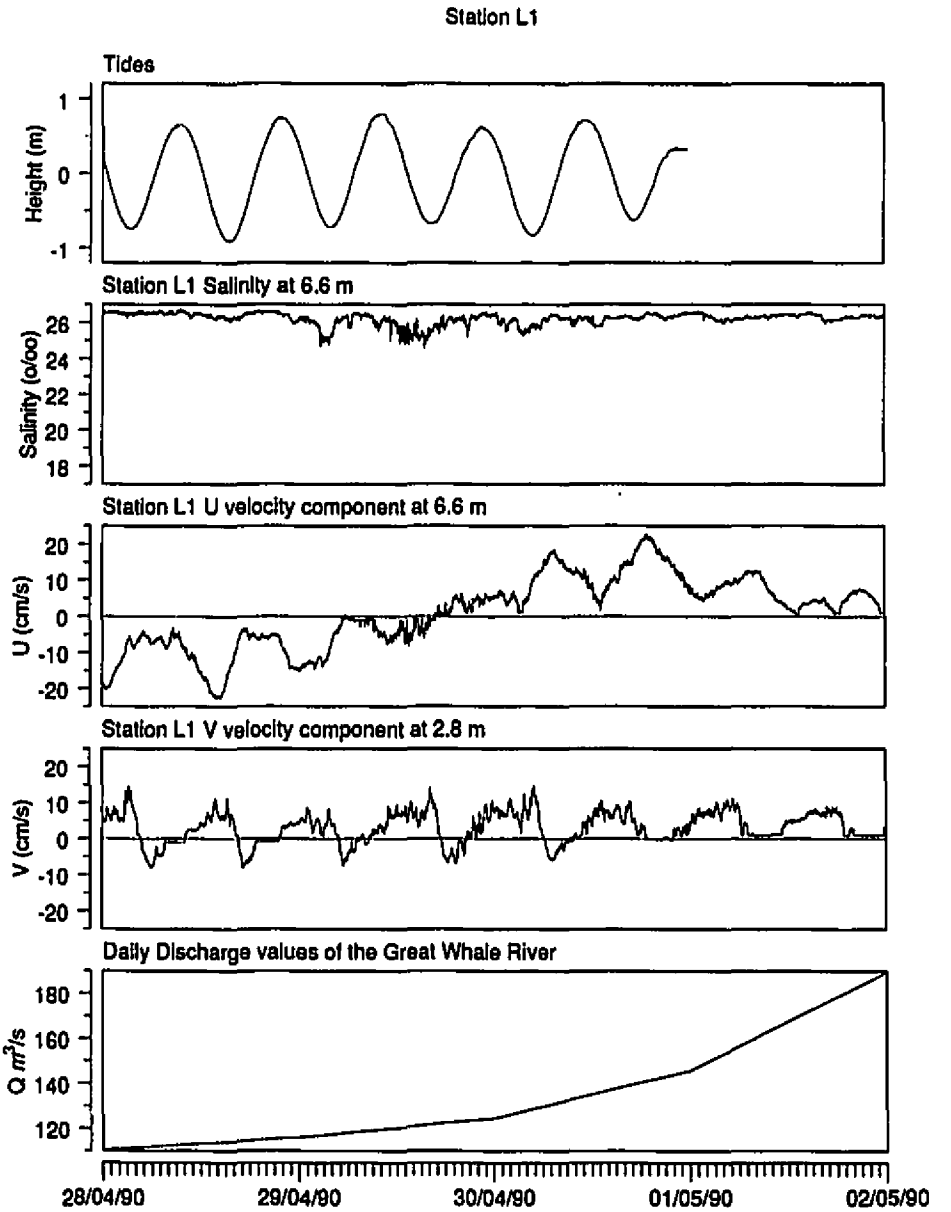

Figure 4.9: RCM data at station L1 for April 28 to May 2, 1990.

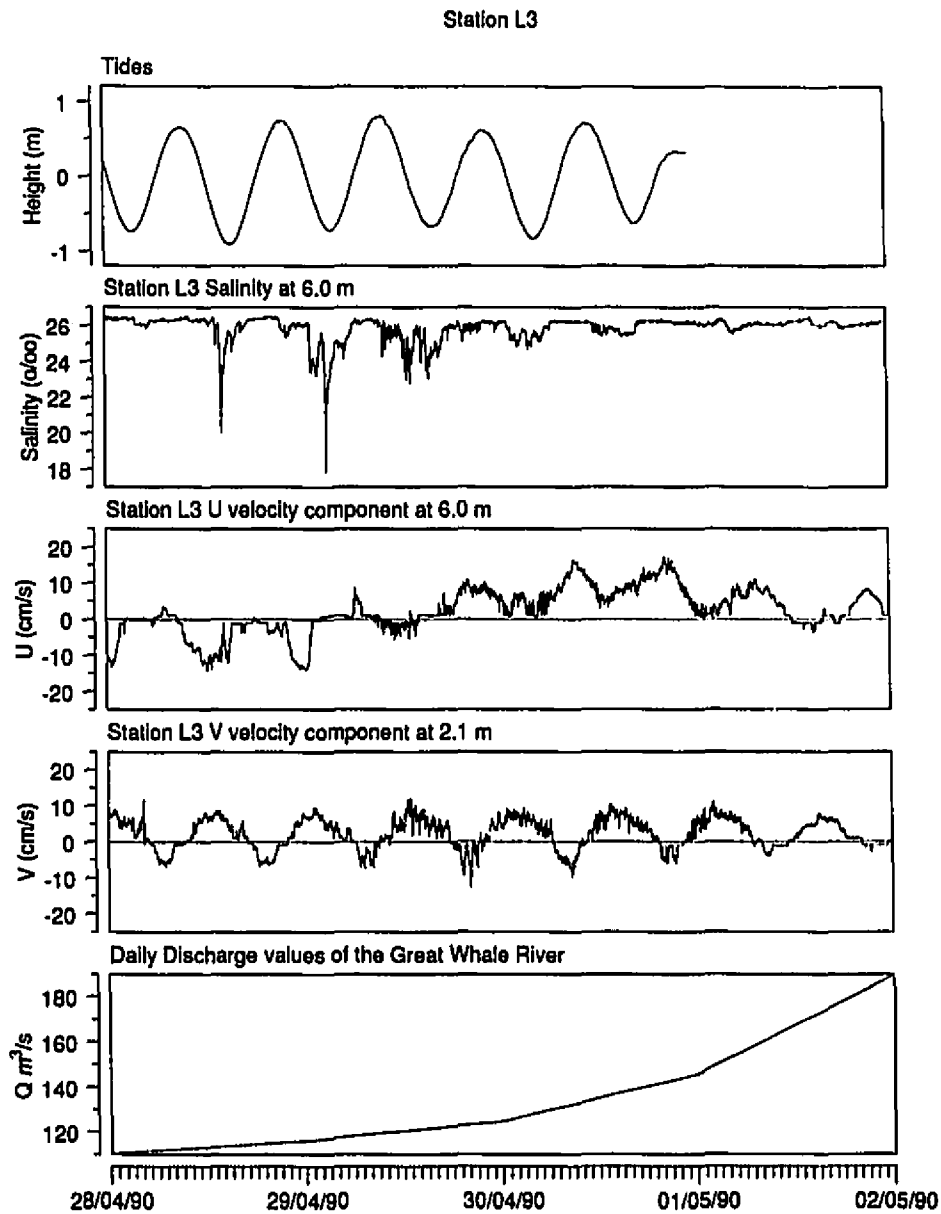

Figure 4.10: RCM data at station L3 for April 28 to May 2, 1990.

in the upper water temperature are apparent with maximum values in the late afternoon. After May 2, the upper level temperatures remain colder than the maximum temperatures attained before this date in the sampling period. This coincides with the increase in freshwater discharge from the Great Whale River. This increase in discharge is due to an increase in ice and snowmelt. There is still a daily cycle of maximum and minimum temperatures. The deeper water readings do not show any notable daily temperature variations, however, there are small fluctuations recorded throughout the day. In Figure 4.7 an increase in the water temperature coincides with a decrease in the salinity, as was discussed earlier.

For this analysis, the coordinate axes for the u and v velocity components have u parallel to the shoreline of Hudson Bay and v perpendicular to it, along the direction of the Great Whale River outflow, as shown in Figure 4.11. The upper level RCM graphs indicate that the v component of the velocity is predominant which corresponds to the Great Whale River outflow, and in the lower levels, the velocity is primarily in the u direction which confirms that the circulation pattern in Hudson Bay is parallel to the shore. Figures 4.5 and 4.7 show low-frequency velocity fluctuations in the u velocity component. Power spectrum analysis of the series gives a period of about three days. Thus, in the Hudson Bay, while the dominant tidal period is semi-diurnal, there are low-frequency fluctuations as well. Reynaud *et al.* (1992) found that the low-frequency variability can be explained by both the average atmospheric pressure

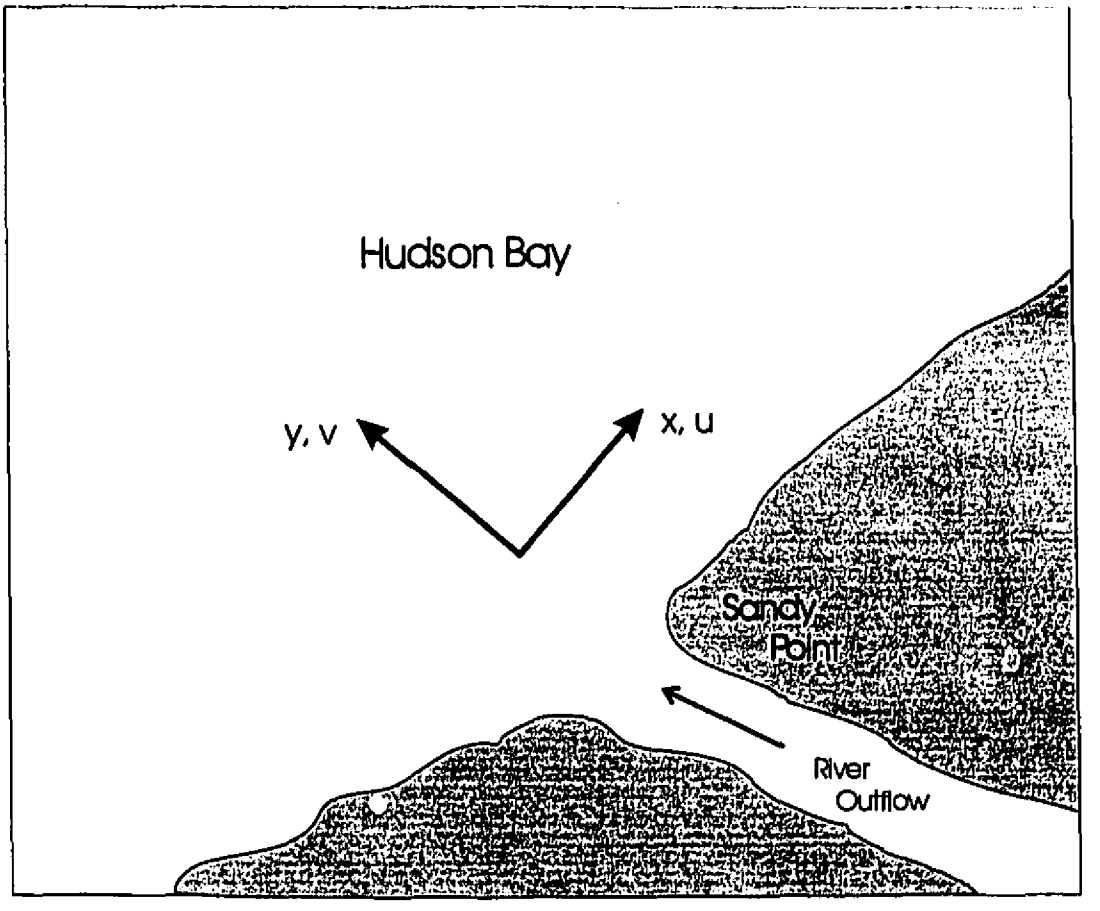

Figure 4.11: u and v coordinate axes for the 1990 RCM data analysis.

and the longshore atmospheric pressure gradient.

To determine the dynamic stability of the water column, the gradient Richardson number (eq. 2.2) was calculated for stations L1 and L3. Stable conditions occurred throughout the sampling period with a minimum value of $Ri = 9.0$ on April 28, 1990. The estuarine Richardson number (eq. 2.4) was evaluated at the mouth of the river. Results for 1988 and 1990 were greater than 1 at the time of the field work. This indicates a strongly stratified system with little mixing.

The internal Froude number calculations (eq.2.6) yielded results much less than 1 at both L1 and L3. This suggests subcritical conditions downstream of the river mouth.

4.4 CTD Data

From the CTD plots, the boundary between the plume water and the Hudson Bay basin water can be easily distinguished by the sharp pycnocline and halocline. Figures 4.12, 4.13, 4.14, 4.15 and 4.16 show salinity, sigma-t and temperature curves with depth for the stations L1 to L5 at high and low tide during spring and neap tides in 1990.

The temperature at L1 is slightly above $0°C$ for the first 3 to 4 m followed by a sharp thermocline and a decrease in temperature to below $-1°C$. Below a depth of about 15 m, there is a slight warming. However, the salinity data do not show

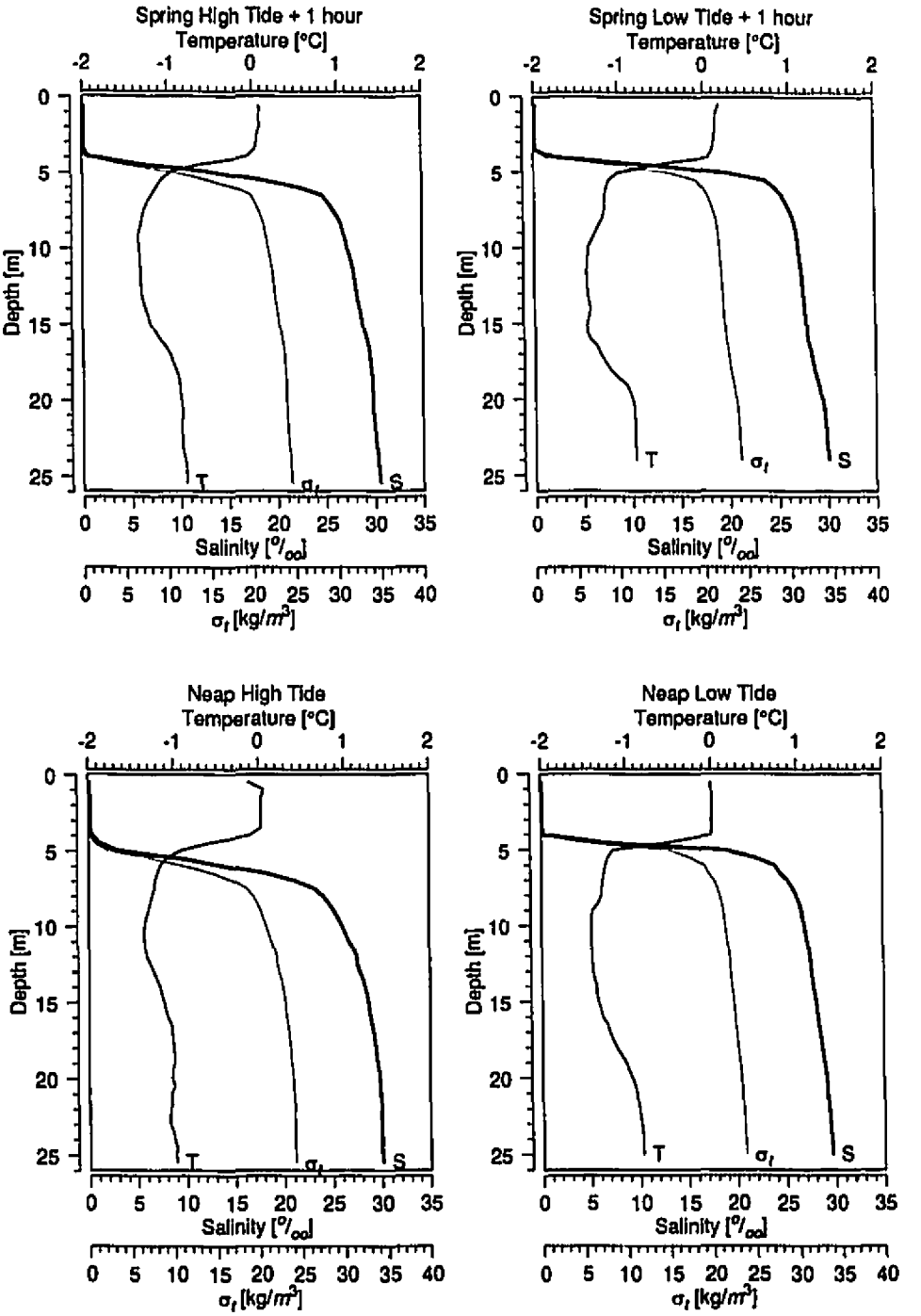

Figure 4.12: CTD data at station L1

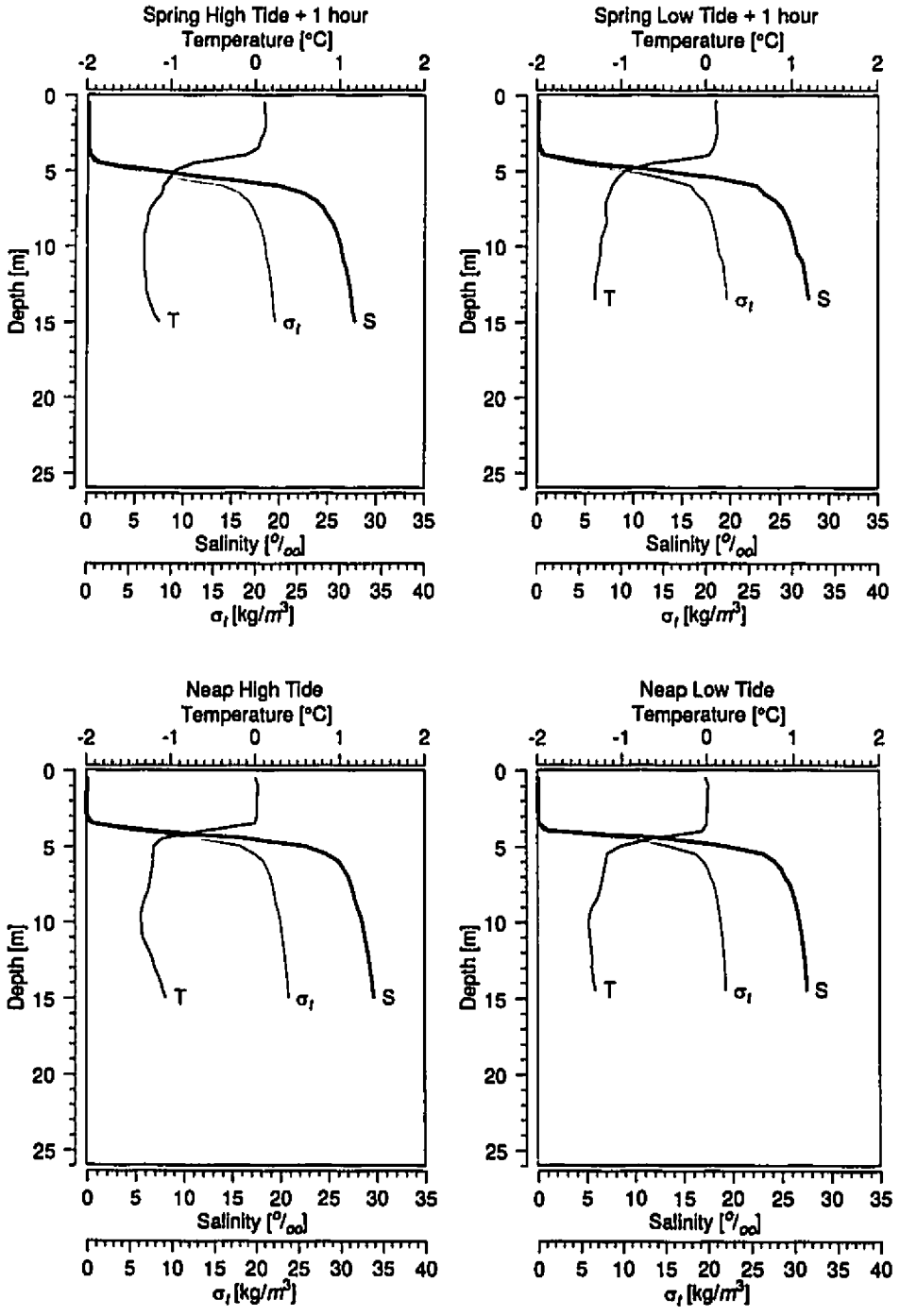

Figure 4.13: CTD data at station L2

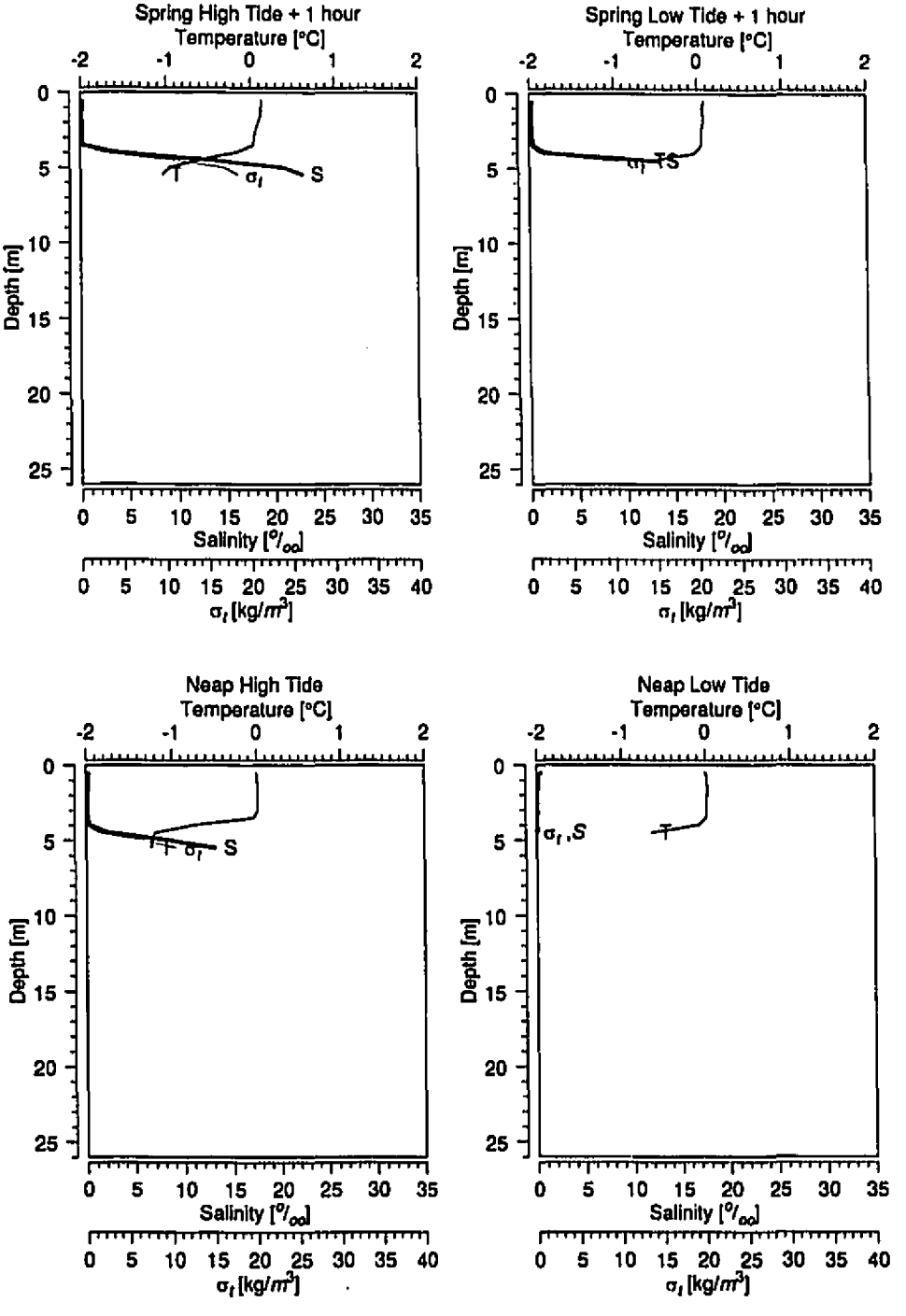

Figure 4.14: CTD data at station L3

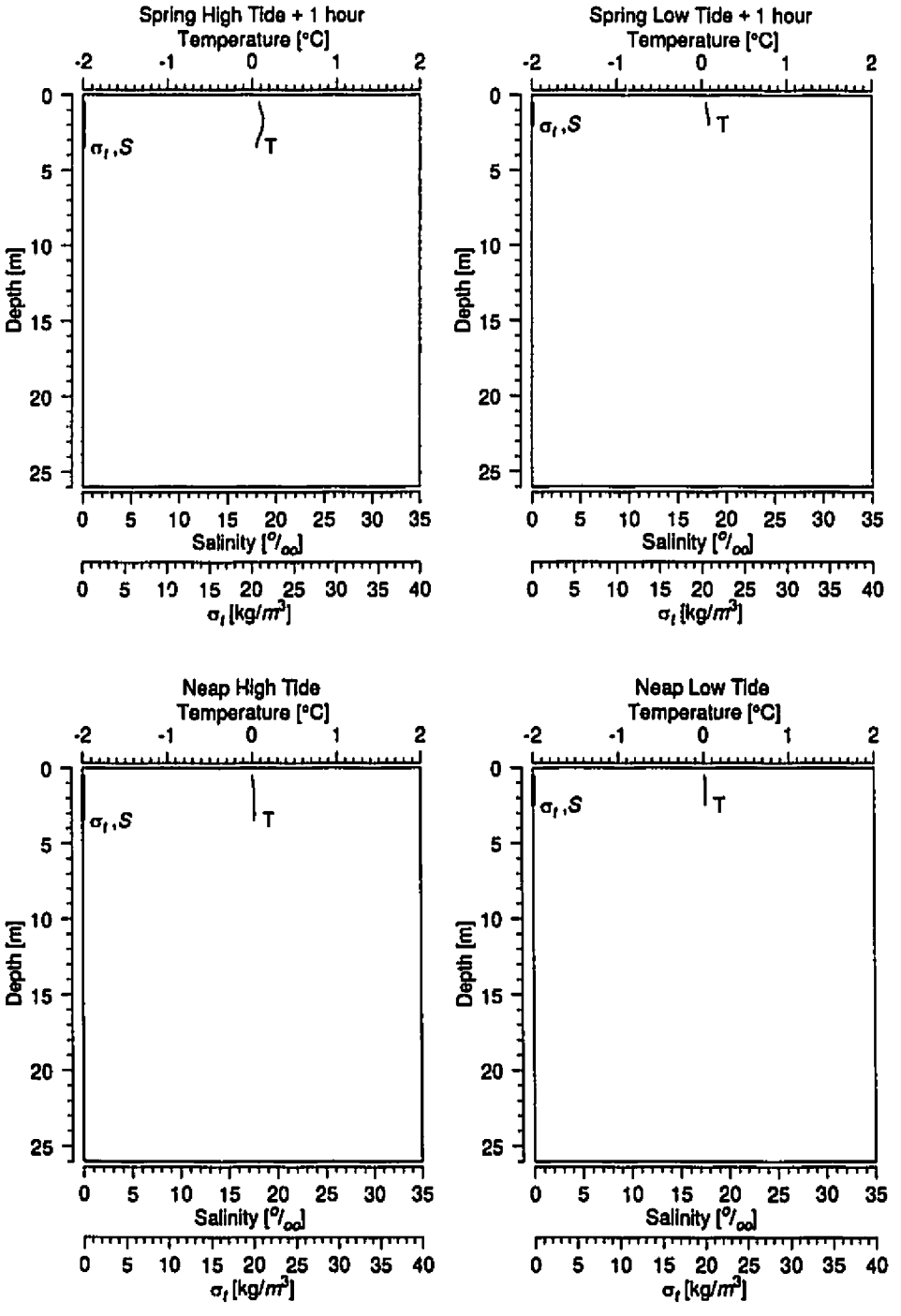

Figure 4.15: CTD data at station L4

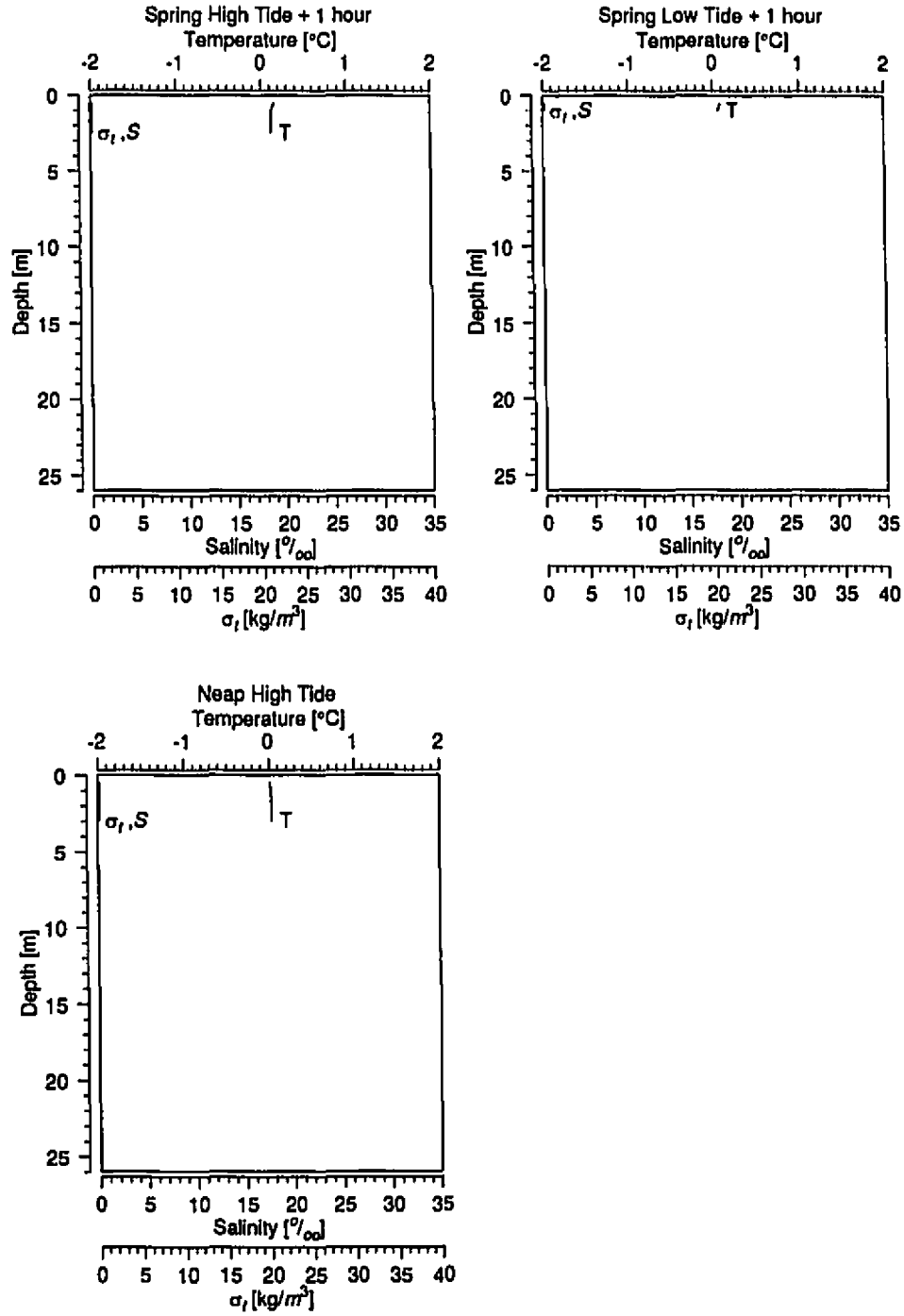

Figure 4.16: CTD data at station L5

a change, indicating that a mass of warmer water with the same salinity as the surrounding Hudson Bay water enters the region. A possible source is the shallower Manitounuk Sound situated to the north of the study area. The salinity and sigma-t curves follow each other, indicating that the salinity has a stronger influence on the density than does the temperature. Sharp haloclines and pycnoclines occur at depths of around 3.5 to 4.0 m. Maximum salinity values are 30 $^{o}/_{oo}$. At station L2, the profiles are similar to those at L1. The depth of the fresh water layer is between 3.5 and 4.0 m. Closer inshore, profiles at station L3 reach only a depth of 5.0 m, which is almost entirely in the fresh water plume region. At neap low tide there was no indication of a pycnocline or halocline. Station L4, with maximum depth of about 3.5 m, is totally in the freshwater plume. Temperatures are $0^{o}C$ and salinity values are 0 $^{o}/_{oo}$. With readings only down to a depth of about 3.0 m at high tide, all that can readily be observed at this station is that salinity values always indicate fresh water.

While these are the patterns most often observed during the period studied, irregular patterns occurred on the afternoon of April 27, 1990, as shown in Figures 4.17 and 4.18.

At 17:20, the freshwater layer increased to a depth of 6.5 m at station L2. A second reading was taken three minutes later and once again a deeper fresh water layer was observed, indicating the possibility of vertical motion. At 17:40, an erosion

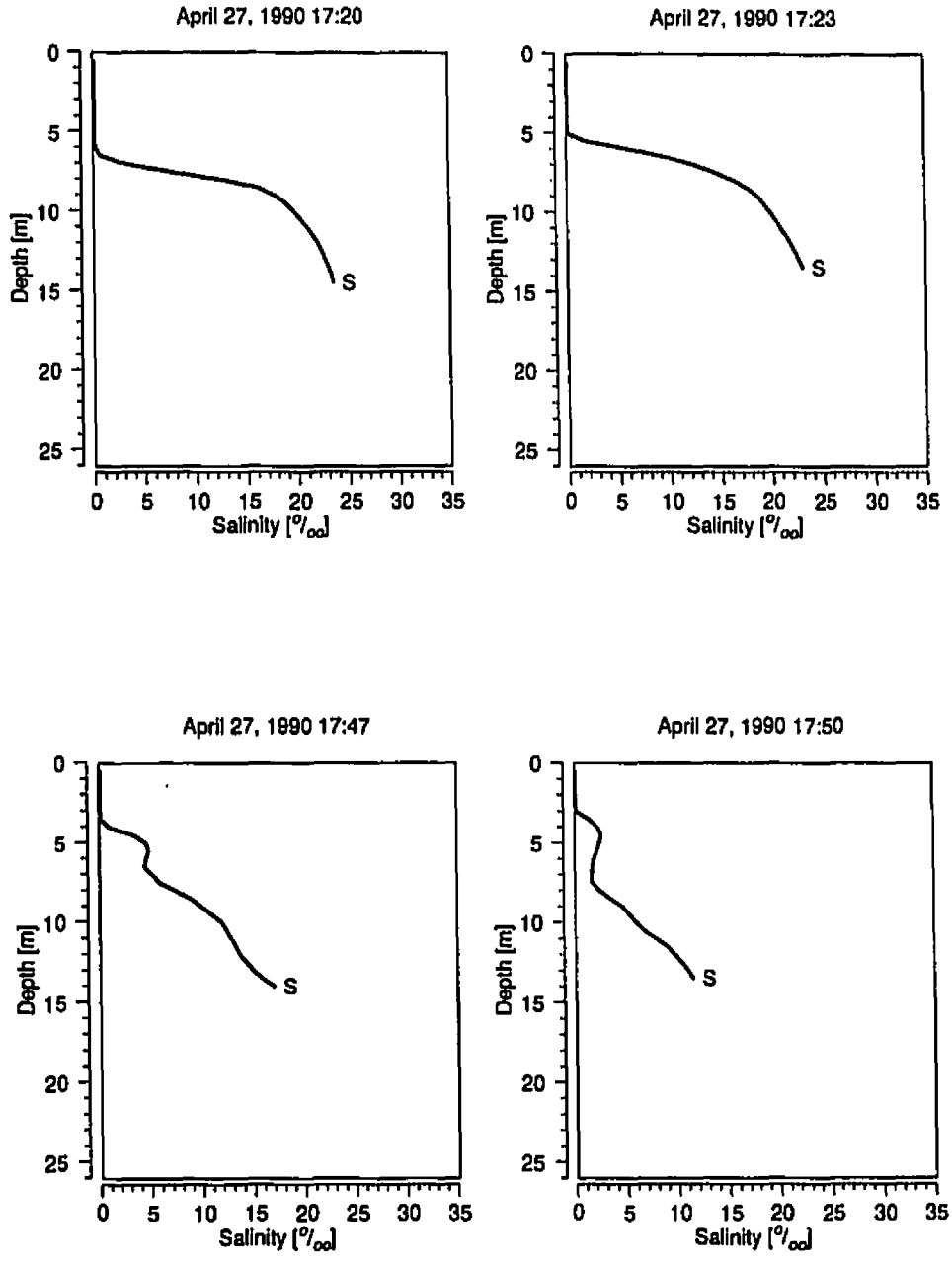

Figure 4.17: Anomalous CTD curves at station L2 taken on April 27, 1990.

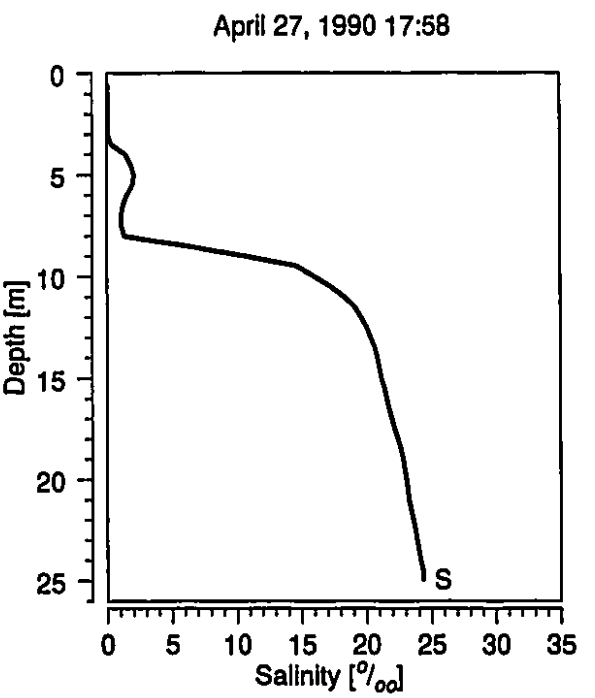

Figure 4.18: Anomalous CTD curve at station L1 taken on April 27, 1990.

of the well defined halocline began. Mixing is defined by Fischer *et al.* (1979) as any process which causes one parcel of water to be mingled with or diluted by another. The salinity values between 4 and 15 m are neither those observed in the freshwater plume layer, nor in the Hudson Bay water in other profiles which suggests mixing. The reading a few minutes later shows a similar pattern at station L1. The measurement taken at 17:58 also indicates a situation in which mixing is occurring. While there were no measurements taken at that station shortly before this event, it is assumed that a deepening of the freshwater layer preceeded it, similar to what was observed at station L2.

4.5 General Flow Pattern

In order to gain further insight into the flow pattern within the 2 km downstream of the river mouth, a vertical cross-section along a line joining the five stations was analysed. From the RCM measurements, the speed and direction of the flow in the freshwater layer and in the Hudson Bay basin could be obtained. The location of the pycnocline was determined from the CTD profiles. Cross-sectional sketches were generated for spring and neap, high and low tides. The spring tide conditions are shown in Figures 4.19 and 4.20, while neap tide conditions are presented in Figures 4.21 and 4.22. The mean flow in the upper layer is always directed outward from the river mouth. The low-frequency variability in the Hudson Bay flow was southward during

the spring tide period and northward at the time of neap tide conditions. The speeds at spring and neap low tide are about the same as are the speeds at spring and neap high tide. Thus, the magnitude of the flow is the same and the direction fluctuates.

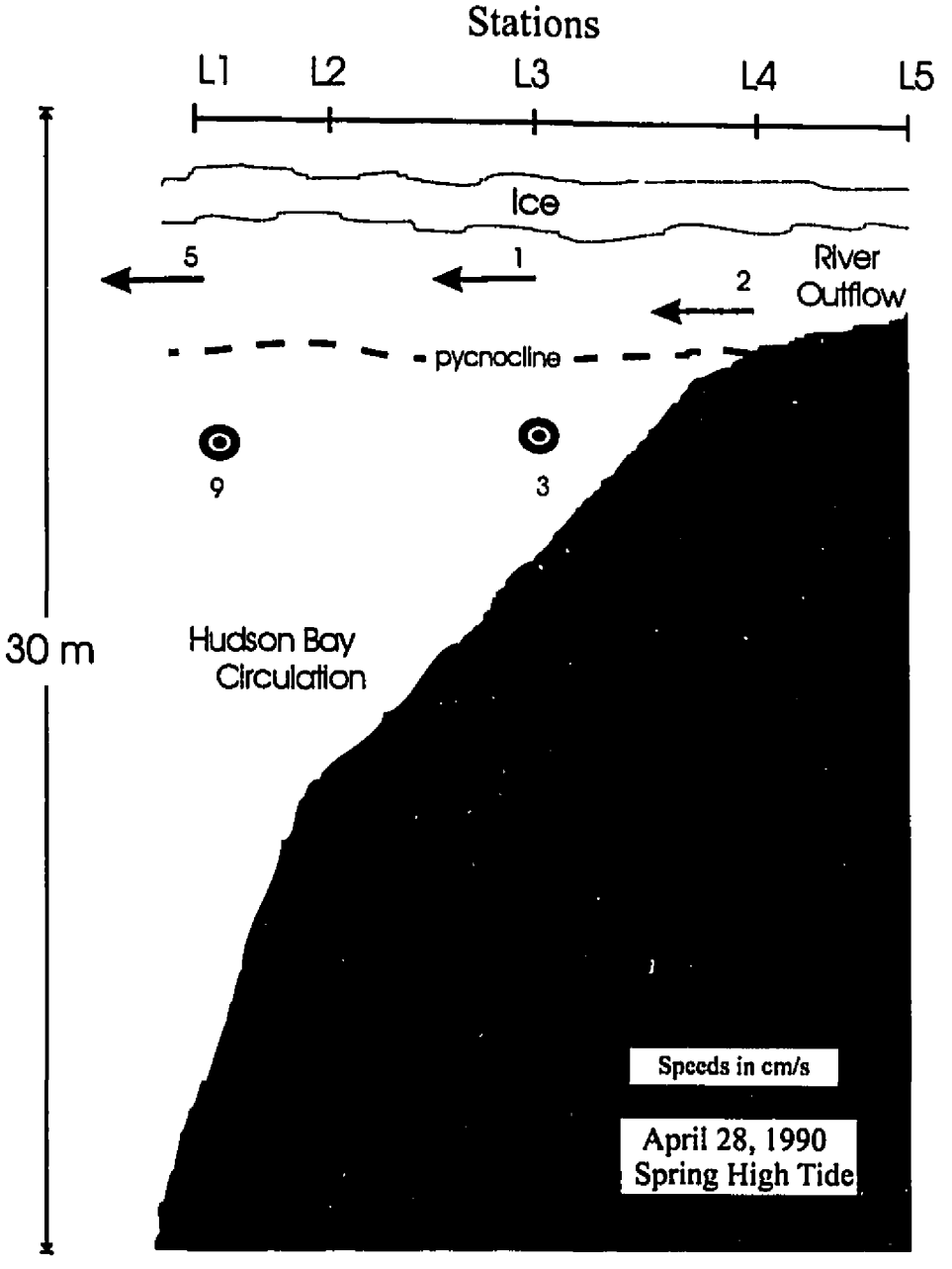

Figure 4.19: Schematic diagram of the cross-section along the sampling transect at spring high tide.

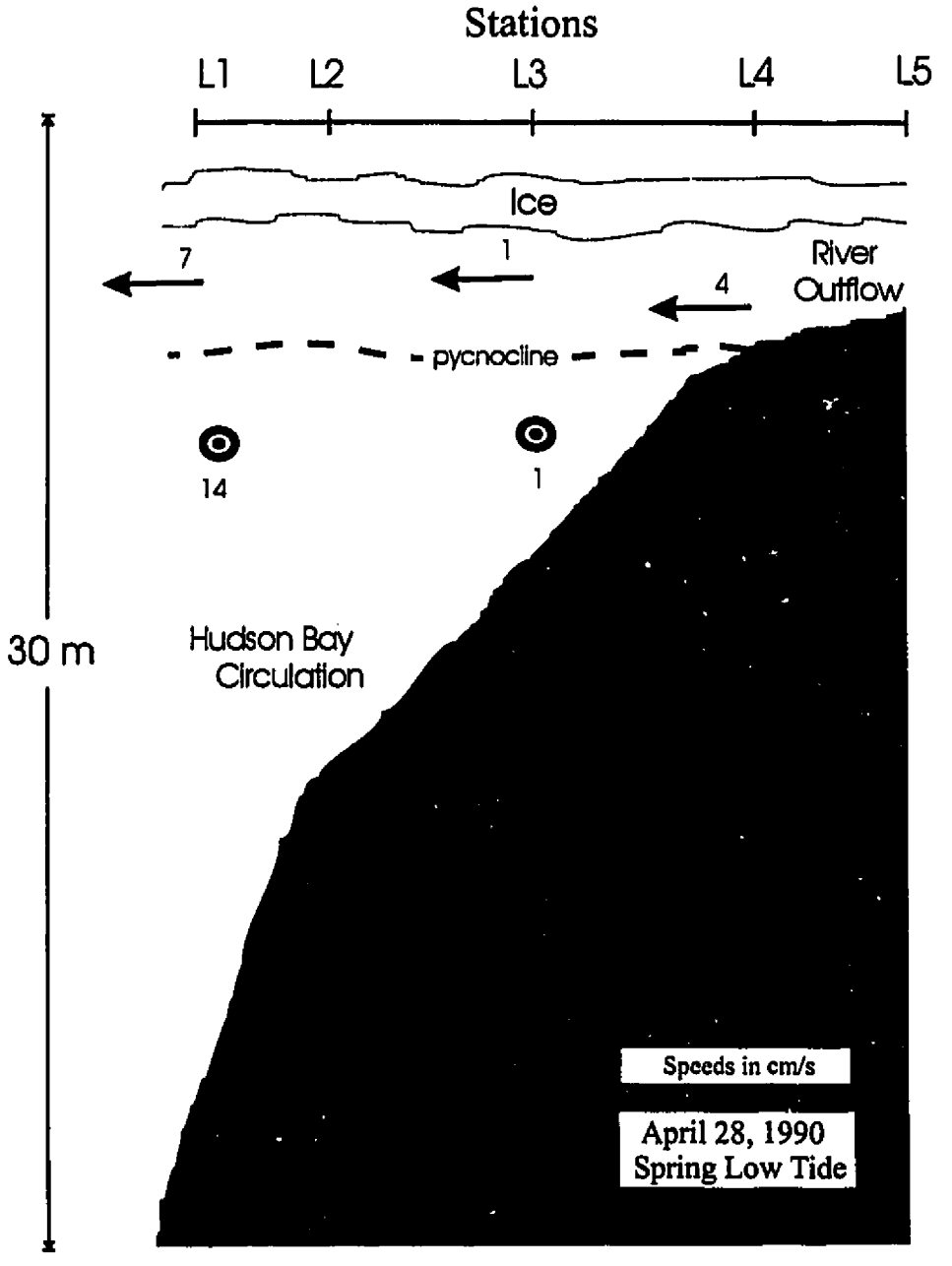

Figure 4.20: Schematic diagram of the cross-section along the sampling transect spring low tide.

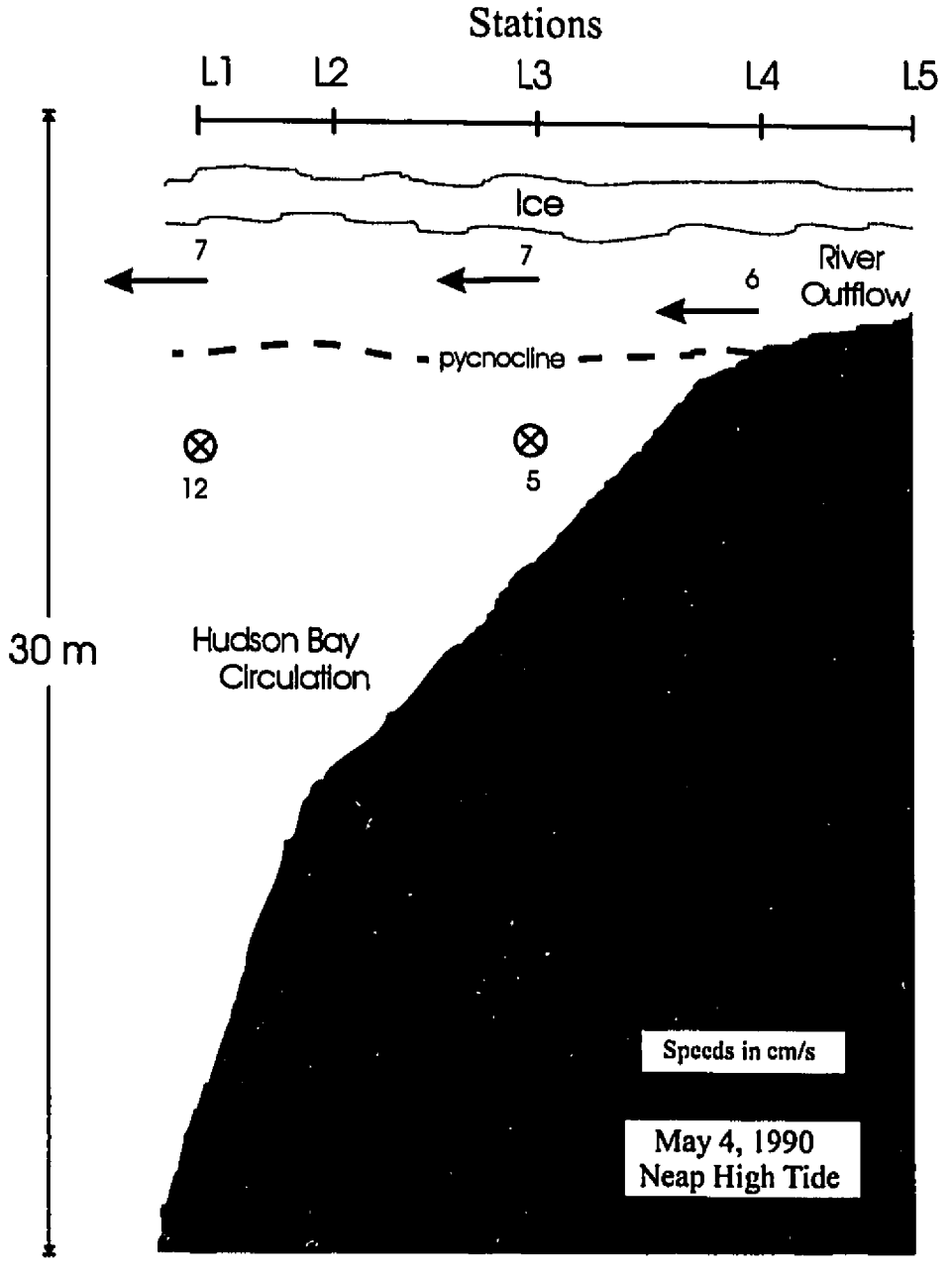

Figure 4.21: Schematic diagram of the cross-section along the sampling transect at neap high tide.

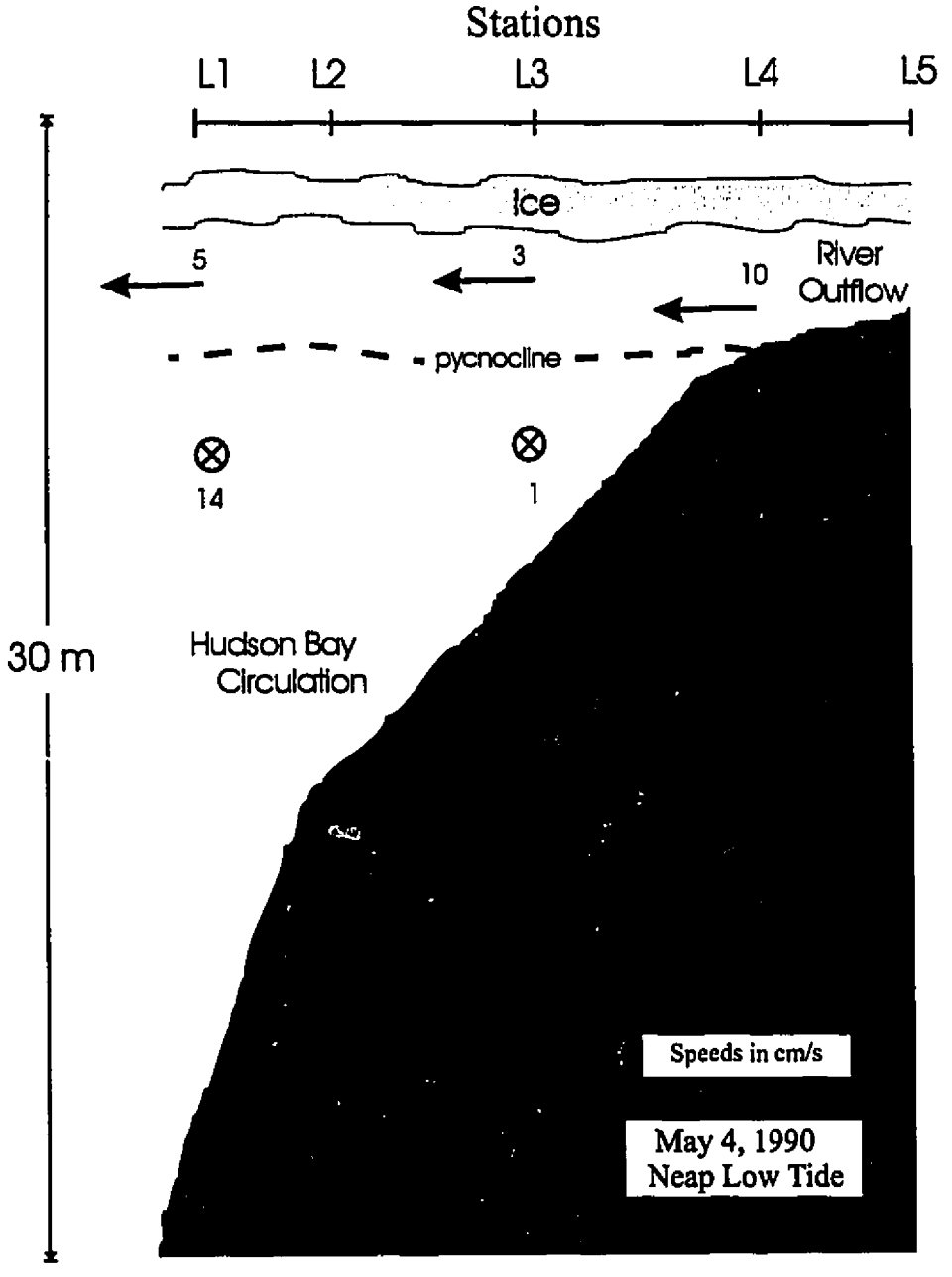

Figure 4.22: Schematic diagram of the cross-section along the sampling transect neap low tide.

Chapter 5

Discussion

5.1 Tides

Tidal analysis of the 1990 data confirmed the work by Godin (1986) and Prinsenberg (1988), since both a damping of the amplitude and a phase advance of the tide were observed. When the predicted tide for 1988 are compared to the analysis of the river mouth RCM data it was found that the maximum velocities occur about four hours after the time of predicted high tide. However, for under-ice conditions one would expect to find this time difference to be even greater due to the phase advance of the tide. This would in fact give the maximum flow speeds closer to the time of low tide.

5.2 Nearshore Conditions

In the previous chapter, the data analysis and results were presented. While the maximum velocity at the river mouth depends both on freshwater discharge and tidal effects, the Ministère de l'Environnement du Québec provides only daily values. This limits the accuracy of the hourly time scale calculations for which discharge values are needed. We assume that the variations over the day were not large. The RCM recordings taken in 1990 indicate that the flow in Hudson Bay is approximately at right angles to the direction of the flow in the plume region immediately offshore of the mouth of the river. Due to the small upper layer speeds, the calculated internal Froude numbers were much less than 1. The large density difference between the lighter upper water and the salty lower water caused very stable conditions, giving large Richardson numbers. The CTD profiles taken in 1990 provide a snapshot of the salinity, temperature and density changes with depth. The patterns showed little variation between high and low tide conditions which suggests the tide has little effect on the plume depth under subcritical conditions. Data collected at the time of the spring low tides in 1990 did not fit the patterns taken at other times during the study period. This event is the subject of the following section.

5.3 Internal Hydraulic Jump

From the RCM measurements taken at L1 and L3 and CTD profiles at L1 and L2, rapid fluctuations in the salinity field were observed between April 27 and 30, 1990. Echosounder data taken at the same time period confirms a fluctuation of the pycnocline depth with the tide. Figures 4.9, 4.10, 4.17 and 4.18 show these events in detail. During the period when the RCM recorded events occurred, no CTD profiles were taken. The events detected in the CTD profiles on April 27, 1990 are not evident in the RCM data at 6.0 m depth. An explanation for this lack of signal is not altogether clear. Perhaps the duration of the anomalous event at the RCM depths was not long enough to be recorded. However, there is strong evidence to suggest the events did occur. One possible explanation is the occurrence of an internal hydraulic jump.

According to Fox and MacDonald (1985), for subcritical flow ($Fr < 1$), the adjustment of the flow to disturbances caused by a change in the slope of the bathymetry or flow in the cross section are smooth. However, when supercritical flow ($Fr > 1$) occurs in a section and downstream conditions require an adjustment to subcritical flow, a gradual change with a smooth transition through the critical point is not possible. The transition may occur abruptly in the form of a hydraulic jump.

Internal Froude numbers calculated at L1 and L3 always were less than 1, indicating subcritical conditions. The observed salinity anomalies occurred on April 27, 28, 29 and 30, 1990, at times which corresponded to the times of lowest low tides during

spring tides. From the echosounder data, it was determined that the surface ice, while being landfast, did indeed move up and down with the tides. Therefore, at the lowest low tides, the depth of the water at the sandbar, the shallowest region through which the water must flow, is greatly reduced. Since the cross-section geometry is far from rectangular, the cross-sectional area is reduced significantly. The reduced area also results in high flow velocities across the mouth at this time. Figure 5.1 shows a schematic diagram of the cross-section over the sandbank for average ice conditions at high tide and during spring low tide.

Since there are no direct current velocity measurements available for 1990, the method discussed in Chapter 4, section 1 was used. The bulk densimetric Froude numbers obtained are given in Table 5.1. Values are greater than 1 indicating supercritical conditions. Figure 5.2 shows the variation of the cross-sectional area, the

Bulk Densimetric Froude Numbers	
Date	**Fr**
April 27, 1990	1.07
April 28, 1990	1.11
April 29, 1990	1.16
April 30, 1990	1.25

Table 5.1: Froude numbers at the mouth of the Great Whale River

river outflow velocity and the Froude number with the tides for April 28, 1990. An ice thickness of 1.5 m was used to obtain these results. If a rectangular cross-section were used, the area through which the water flows would be much larger resulting

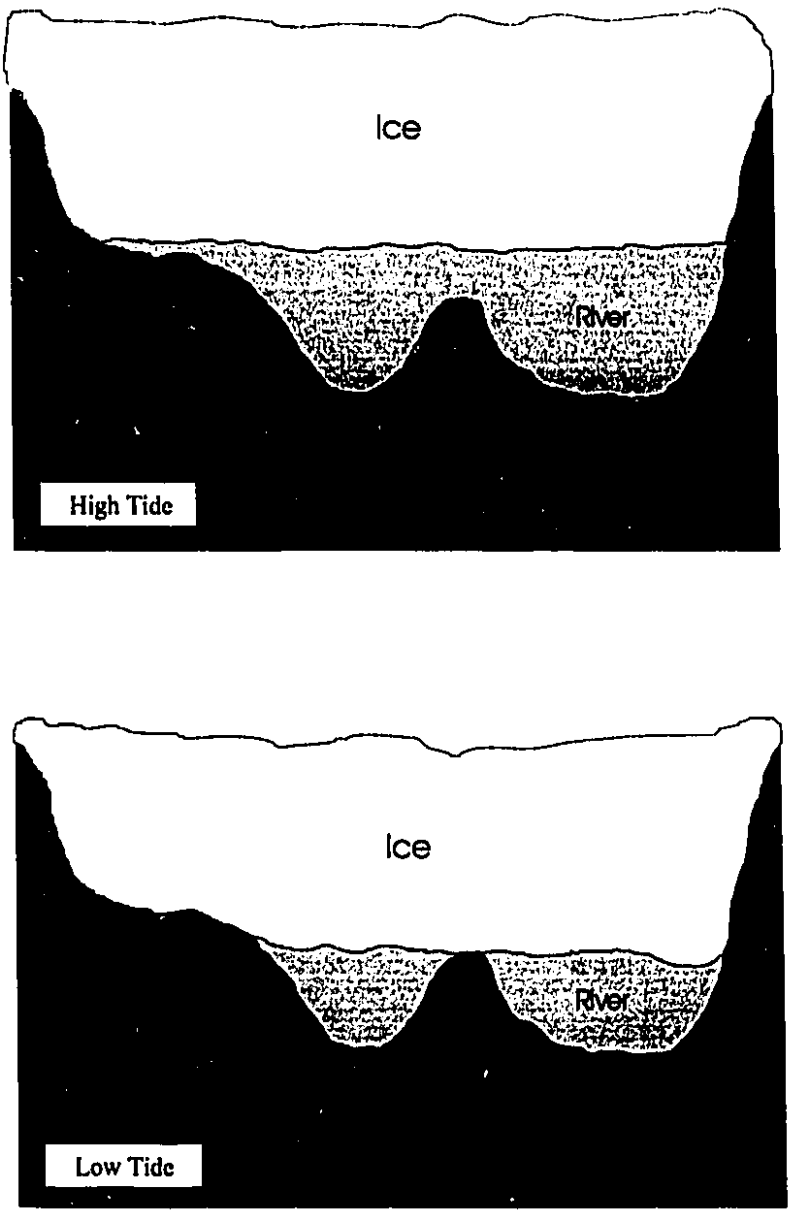

Figure 5.1: Schematic diagram of the cross-section over the sandbar at average high tide and at spring low tide.

in lower velocities. The maximum densimetric Froude number would be about 0.5, which implies subcritical conditions. These calculations only consider the decrease in area due to tidal fluctuations. Frazil ice formation (Hydro Québec, personal communication) could further decrease the area, thus increasing the discharge velocity and resulting in even larger Froude numbers. The formation of frazil ice is a function of the velocity. For stronger flow, the growth of frazil ice increases. Average frazil ice thicknesses of 4 to 5 m were measured 5 km upriver from the mouth of the Great Whale River (Hydro Québec, personal communication).

From the monthly mean values of the discharge from the Great Whale River (Figure 3.2), it is apparent that the maximum runoff does not occur at the same time every year. In 1988, values of 1200 m^3/s occurred in early May, which are much higher than those at the same time of the year in 1990. If one made the assumption that all the conditions are the same as those described above, but took a discharge value of 1200 m^3/s, then a minimum densimetric Froude number of 5 was calculated for spring high tide conditions. Thus, as the rate of discharge increases, supercritical conditions become possible, even at high tide. This would produce a thicker freshwater layer. However, with higher river outflow, the mean level of the water would rise slightly as well and would increase the outflow area. If an increase of 0.5 m in the water level were assumed, spring high tide Froude numbers would be less than 1. However, at neap high tide, conditions would still be supercritical. Analysis of the 1988 Great

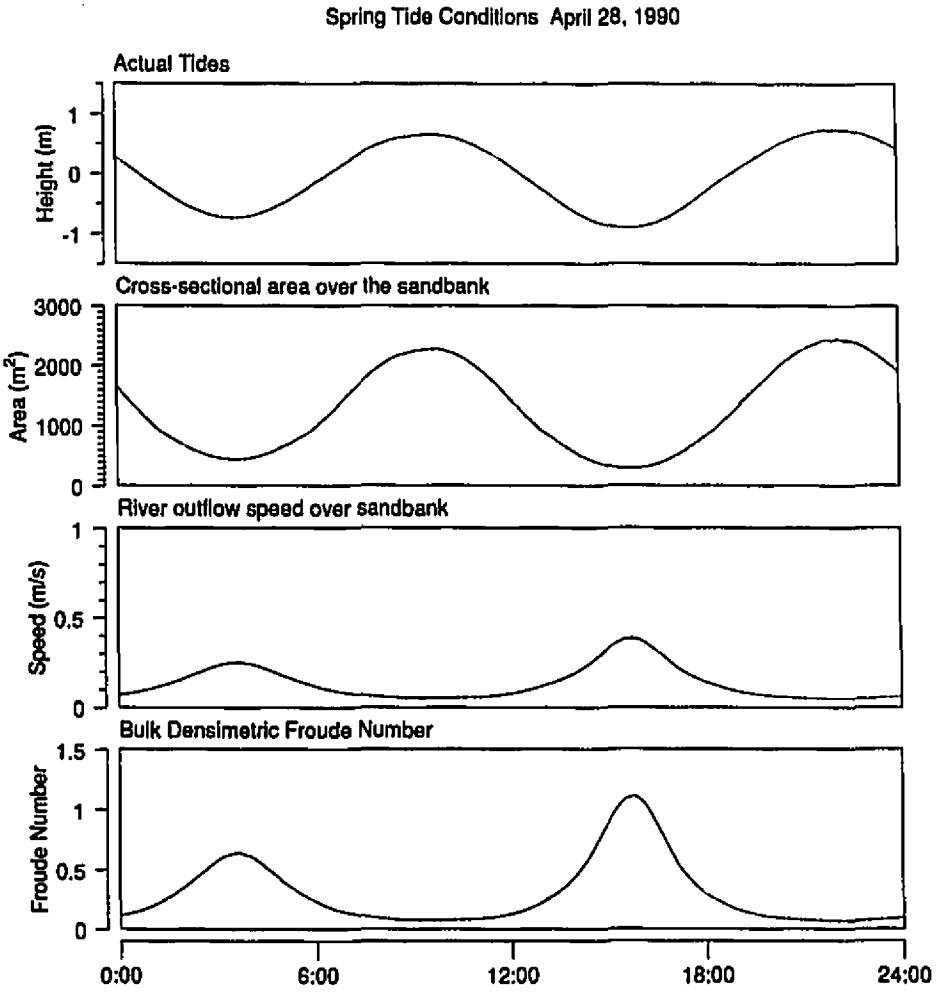

Figure 5.2: Tides, cross-sectional areas, river outflow speeds and Froude numbers for April 28, 1990.

Whale River plume was carried out by Veilleux (1990). The river velocities were calculated using the same method used in this analysis, however, values were less than expected for the high flow conditions. One explanation for this is that the area she used was not over the sandbank but rather in a deeper area of the river mouth and the change in outflow area due to the rise and fall of the ice cover with the tides was not considered.

Chapter 6

Conclusions

Previous plume studies (Chao and Boicourt, 1986), (Chao, 1988a; 1988b; 1990), (Freeman, 1982), (Garvine, 1974; 1977; 1982; 1987), (Ingram, 1981; 1987), (Lepage and Ingram, 1991), (Luketina and Imberger, 1987), and(O'Donnell, 1990) have considered the plume as a whole, with a focus on its leading edge and the fronts that may or may not be present. The purpose of this work was to provide a clearer understanding of the nearshore characteristics of an under-ice river plume. The time period over which data was collected in both 1988 and 1990 was early spring, providing a complete ice covered offshore yet increasing river discharge because of the thaw on land.

The general characteristics of the plume in the first 2 km from the river mouth were determined using the continuous data record obtained from the RCMs, the profiles of the CTD and echosounder readings. Stations L4 and L5 were located in shallow

water, therefore all measurements were taken solely in the fresh plume water region. Stations L1, L2 and L3 were situated further offshore resulting in observations being taken in the fresh water region and the saltier Hudson Bay water.

The nearshore characteristics were determined. The river outflow velocities vary depending on the river discharge and the tides. The first several hundred meters from the river mouth are characterized by freshwater. At a distance of 1.5 km offshore, we see evidence for Hudson Bay waters. From the CTD profiles, the depth of the pycnocline is between 4.0 and 4.5 m at all five stations. Calculations of the Richardson number and the internal Froude number at the offshore stations suggest stable, subcritical conditions. The general pattern in the nearshore region did not always have similar characteristics. During the spring tides of April 1990, short-lived perturbations to the depth of the freshwater upper layer occurred. Froude number calculations at the river mouth indicated supercritical conditions which strengthens the assertion that an internal hydraulic jump formed at this time. Nearshore analysis of flow conditions at other rivers would be useful. If internal hydraulic jumps, or the deepening of the freshwater layer occur more frequently or even regularly during certain discharge conditions, there could be significant biological consequences.

References

BADDOUR, R. E. AND CHU, V. H. (1975). Buoyant surface discharge on a step and on a sloping bottom. Report 75-2, Fluid Mechanics Laboratory McGill University, Montreal, 57 pages.

BEARMAN, G. (1989). *Waves, Tides and Shallow Water Processes.* Pergamon Press, New York, 187 pages.

BO PEDERSEN, F. (1987). *Lecture Notes on Coastal and Estuarine Studies - Environmental Hydraulics : Stratified Flows*, volume 18. Springer-Verlag, New York, 278 pages.

BOWDEN, K. F. (1983). *Physical Oceanography of Coastal Waters.* Halsted Press, New York, 302 pages.

BOWMAN, M. J. AND IVERSON, R. L. (1977). Estuarine and plume fronts. In BOWMAN, M. J. AND ESAIAS, W. E., editors, *Oceanic Fronts in Coastal Processes*, pages 87–104, New York. Springer-Verlag.

Canadian Tide and Current Tables (1988). *Arctic and Hudson Bay*, volume 4. Fisheries and Oceans Canada.

Canadian Tide and Current Tables (1990). *Arctic and Hudson Bay*, volume 4. Fisheries and Oceans Canada.

CHAO, S. (1988a). River forced estuarine plumes. *J. Phys. Oceanogr.*, 18:72–88.

CHAO, S. (1988b). Wind driven motion of estuarine plumes. *J. Phys. Oceanogr.*, 18:1144–1166.

CHAO, S. (1990). Tidal modulation of estuarine plumes. *J. Phys. Oceanogr.*, 20:1115–1123.

CHAO, S. AND BOICOURT, W. (1986). Onset of estuarine plumes. *J. Geophys. Res.*, 16:2237–2149.

CHU, V. H. AND JIRKA, G. H. (1986). *Encyclopedia of Fluid Mechanics*, volume 6, chapter 25, pages 357–373. Gulf Publishing, Houston.

ELLISON, T. H. AND TURNER, J. S. (1959). Turbulent entrainment in stratified flows. *J. Fluid Mech.*, 6:423–448.

FISCHER, H. B., LIST, E. J., KOH, R., IMBERGER, J., AND BROOKS, N. H. (1979). *Mixing in Inland and Coastal Waters.* Academic Press, New York, 483 pages.

FORRESTER, W. D. (1983). *Canadian Tidal Manual.* Government of Canada, Fisheries and Oceans, Ottawa, 138 pages.

FORTIER, L., GILBERT, M., PONTON, D., INGARM, R. G., ROBINEAU, B., AND LEGENDRE, L. (1995). Impact of freshwater on subarctic coastal ecosystem under seasonal sea ice (southeastern Hudson bay, canada).III. Feeding success of marine fish larvae. *in press.*

FOX, R. W. AND MCDONALD, A. T. (1985). *Introduction to Fluid Mechanics.* John Wiley and Sons, Toronto, 741 pages, 3 edition.

FREEMAN, N. G. (1982). *Measurement and Modelling of Freshwater Plumes Under an Ice Cover.* Ph.D. thesis, University of Waterloo, Waterloo, Canada, 155 pages.

GARVINE, R. W. (1974). Physical features of the Connecticut River outflow during high discharge. *J. Geophys. Res.*, 79:831–846.

GARVINE, R. W. (1977). Observations of the motion field of the Connecticut River plume. *J. Geophys. Res.*, 82:441–454.

GARVINE, R. W. (1982). A steady state model for buoyant surface plume hydrodynamics in coastal waters. *Tellus*, 34:293–306.

GARVINE, R. W. (1987). Estuary plume fronts in shelf waters : A layer model. *J. Phys. Oceanogr.*, 17:1877–1896.

GILBERT, M., FORTIER, L., PONTON, D., AND DROLET, R. (1992). Feeding ecology of marine fish larvae across the Great Whale River plume in seasonally ice-covered southeastern Hudson Bay. *Mar. Ecol. Prog. Ser.*, 84:19–30.

GODIN, G. (1986). Modification by an ice cover of the tide in James Bay and Hudson Bay. *Arctic*, 39:65–67.

INGRAM, R. G. (1981). Characteristics of the Great Whale River plume. *J. Geophys. Res.*, 86:2017–1023.

INGRAM, R. G. AND LAROUCHE, P. (1987a). Changes in the under-ice characteristics of La Grande Rivière plume due to discharge variation . *Atmosphere-Ocean*, 25:242–250.

INGRAM, R. G. AND LAROUCHE, P. (1987b). Variability of an under ice river plume in Hudson Bay. *J. Geophys. Res.*, 92:9541-9547.

KRANENBURG, C. (1987). Boundary induced entrainment in two-layer stratified flow. *J. Geophys. Res.*, 92:5417–5425.

KUNDU, P. K. (1990). *Fluid Mechanics*. Academic Press, San Diego, 638 pages.

LAROUCHE, P. AND GALBRAITH, P. S. (1989). Factors affecting east-ice consolidation in southeastern Hudson Bay, Canada. *Atmosphere-Ocean*, 27:367–375.

LEPAGE, S. AND INGRAM, R. G. (1991). Variation of upper layer dynamics during breakup of the seasonal ice cover in Hudson Bay. *J. Geophys. Res.*, 96:12711–12724.

LUKETINA, D. A. AND IMBERGER, J. (1987). Characteristics of a surface buoyant jet. *J. Geophys. Res.*, 92:5435–5447.

LUKETINA, D. A. AND IMBERGER, J. (1989). Turbulence and entrainment in a buoyant surface plume. *J. Geophys. Res.*, 94:12 619–12 636.

MESSIER, D., LEPAGE, S., AND DE MARGERIE, S. (1989). Influence du couvert de glace sur l' étendue du panache de la Grande Rivière (Baie James). *Arctic*, 42:278–284.

O'DONNELL, J. (1990). The formation and fate of a river plume : A numerical model. *J. Phys. Oceanogr.*, 20:551–569.

OFFICER, C. B. (1976). *Physical Oceanography of Estuaries and Associated Coastal Waters*. John Wiley and Sons, Toronto, 465 pages.

POND, S. AND PICKARD, G. L. (1983). *Introductory Dynamical Oceanography*. Pergamon Press, New York, 329 pages, 2 edition.

PRINSENBERG, S. J. (1987). Seasonal current variations observed in western Hudson Bay. *J. Geophys. Res.*, 92:10 756–10 766.

PRINSENBERG, S. J. (1988). Damping and phase advance in the tide in western Hudson Bay by the annual ice cover. *J. Phys. Oceanogr.*, 18:1744–1751.

PRINSENBERG, S. J. AND FREEMAN, N. G. (1986). *Canadian Inland Seas*, chapter 11, pages 205-216. Elsevier Science, New York.

REYNAUD, T. AND R. G. INGRAM, H. J. FREELAND, A. J. W. (1992). Propagation of coastal-trapped waves under an ice cover in Hudson Bay. *Atmosphere-Ocean*, 30:593-620.

SAFAIE, B. (1979). Mixing of buoyant surface jet over sloping bottom. *J. of the Waterway Port coastal and Ocean Division*, WW4:357-373.

STRILAEFF, P. W. AND BILOZOR, W. (1973). Single-velocity method in measuring discharge. Report 75, Inland Waters Directorate, Water Resources Branch, Ottawa, Canada, 21 pages.

VEILLEUX, L. (1990). Physical Oceanography of Northern Estuaries. Master's thesis, Department of Atmospheric and Oceanic Sciences, McGill University, Montreal, Canada, 109 pages.